70. Bett JS, Goellner GM, Woodman B, Pratt G, Rechsteiner M, Bates GP (2006) Proteasome impairment does not contribute to pathogenesis in R6/2 Huntington's disease mice: exclusion of proteasome activator REG{gamma} as a therapeutic target. Hum Mol Genet 15:33–44
71. Yamamoto A, Lucas JJ, Hen R (2000) Reversal of neuropathology and motor dysfunction in a conditional model of Huntington's disease. Cell 101:57–66
72. Zu T, Duvick LA, Kaytor MD, Berlinger MS, Zoghbi HY, Clark HB, Orr HT (2004) Recovery from polyglutamine-induced neurodegeneration in conditional SCA1 transgenic mice. J Neurosci 24:8853–8861
73. Chen HK, Fernandez-Funez P, Acevedo SF, Lam YC, Kaytor MD, Fernandez MH, Aitken A, Skoulakis EM, Orr HT, Botas J, Zoghbi HY (2003) Interaction of Akt-phosphorylated ataxin-1 with 14-3-3 mediates neurodegeneration in spinocerebellar ataxia type 1. Cell 113:457–468
74. Koprivica V, Cho KS, Park JB, Yiu G, Atwal J, Gore B, Kim JA, Lin E, Tessier-Lavigne M, Chen DF, He Z (2005) EGFR activation mediates inhibition of axon regeneration by myelin and chondroitin sulfate proteoglycans. Science 310:106–110
75. Herrmann O, Baumann B, de Lorenzi R, Muhammad S, Zhang W, Kleesiek J, Malfertheiner M, Kohrmann M, Potrovita I, Maegele I, Beyer C, Burke JR, Hasan MT, Bujard H, Wirth T, Pasparakis M, Schwaninger M (2005) IKK mediates ischemia-induced neuronal death. Nat Med 11:1322–1329
76. Bagatell R, Paine-Murrieta GD, Taylor CW, Pulcini EJ, Akinaga S, Benjamin IJ, Whitesell L (2000) Induction of a heat shock factor 1-dependent stress response alters the cytotoxic activity of hsp90-binding agents. Clin Cancer Res 6:3312–3318
77. Murakami Y, Uehara Y, Yamamoto C, Fukazawa H, Mizuno S (1991) Induction of hsp 72/73 by herbimycin A, an inhibitor of transformation by tyrosine kinase oncogenes. Exp Cell Res 195:338–344
78. Zou J, Guo Y, Guettouche T, Smith DF, Voellmy R (1998) Repression of heat shock transcription factor HSF1 activation by HSP90 (HSP90 complex) that forms a stress-sensitive complex with HSF1. Cell 94:471–480
79. Rokutan K, Hirakawa T, Teshima S, Nakano Y, Miyoshi M, Kawai T, Konda E, Morinaga H, Nikawa T, Kishi K (1998) Implications of heat shock/stress proteins for medicine and disease. J Med Investig 44:137–147
80. Warrick JM, Chan HY, Gray-Board GL, Chai Y, Paulson HL, Bonini NM (1999) Suppression of polyglutamine-mediated neurodegeneration in Drosophila by the molecular chaperone HSP70. Nat Genet 23:425–428
81. Wyttenbach A, Carmichael J, Swartz J, Furlong RA, Narain Y, Rankin J, Rubinsztein DC (2000) Effects of heat shock, heat shock protein 40 (HDJ-2), and proteasome inhibition on protein aggregation in cellular models of Huntington's disease. Proc Natl Acad Sci U S A 97:2898–2903
82. Katsuno M, Sang C, Adachi H, Minamiyama M, Waza M, Tanaka F, Doyu M, Sobue G (2005) Pharmacological induction of heat-shock proteins alleviates polyglutamine-mediated motor neuron disease. Proc Natl Acad Sci U S A 102:16801–16806
83. Hay DG, Sathasivam K, Tobaben S, Stahl B, Marber M, Mestril R, Mahal A, Smith DL, Woodman B, Bates GP (2004) Progressive decrease in chaperone protein levels in a mouse model of Huntington's disease and induction of stress proteins as a therapeutic approach. Hum Mol Genet 13:1389–1405
84. Agrawal N, Pallos J, Slepko N, Apostol BL, Bodai L, Chang LW, Chiang AS, Thompson LM, Marsh JL (2005) Identification of combinatorial drug regimens for treatment of Huntington's disease using Drosophila. Proc Natl Acad Sci U S A 102:3777–3781
85. Dou F, Netzer WJ, Tanemura K, Li F, Hartl FU, Takashima A, Gouras GK, Greengard P, Xu H (2003) Chaperones increase association of tau protein with microtubules. Proc Natl Acad Sci U S A 100:721–726
86. Petrucelli L, Dickson D, Kehoe K, Taylor J, Snyder H, Grover A, De Lucia M, McGowan E, Lewis J, Prihar G, Kim J, Dillmann WH, Browne SE, Hall A, Voellmy R, Tsuboi Y, Dawson TM, Wolozin B, Hardy J, Hutton M (2004) CHIP and Hsp70 regulate tau ubiquitination, degradation and aggregation. Hum Mol Genet 13:703–714
87. Benussi L, Ghidoni R, Paterlini A, Nicosia F, Alberici AC, Signorini S, Barbiero L, Binetti G (2005) Interaction between tau and alpha-synuclein proteins is impaired in the presence of P301L tau mutation. Exp Cell Res 308:78–84
88. Auluck PK, Bonini NM (2002) Pharmacological prevention of Parkinson disease in Drosophila. Nat Med 8:1185–1186
89. Auluck PK, Meulener MC, Bonini NM (2005) Mechanisms of suppression of {alpha}-synuclein neurotoxicity by geldanamycin in Drosophila. J Biol Chem 280:2873–2878
90. Flower TR, Chesnokova LS, Froelich CA, Dixon C, Witt SN (2005) Heat shock prevents alpha-synuclein-induced apoptosis in a yeast model of Parkinson's disease. J Mol Biol 351: 1081–1100
91. Lu A, Ran R, Parmentier-Batteur S, Nee A, Sharp FR (2002) Geldanamycin induces heat shock proteins in brain and protects against focal cerebral ischemia. J Neurochem 81:355–364
92. Giffard RG, Xu L, Zhao H, Carrico W, Ouyang Y, Qiao Y, Sapolsky R, Steinberg G, Hu B, Yenari MA (2004) Chaperones, protein aggregation, and brain protection from hypoxic/ischemic injury. J Exp Biol 207:3213–3220
93. Murphy P, Sharp A, Shin J, Gavrilyuk V, Dello Russo C, Weinberg G, Sharp FR, Lu A, Heneka MT, Feinstein DL (2002) Suppressive effects of ansamycins on inducible nitric oxide synthase expression and the development of experimental autoimmune encephalomyelitis. J Neurosci Res 67:461–470
94. Xiao N, Callaway CW, Lipinski CA, Hicks SD, DeFranco DB (1999) Geldanamycin provides posttreatment protection against glutamate-induced oxidative toxicity in a mouse hippocampal cell line. J Neurochem 72:95–101
95. Sano M (2001) Radicicol and geldanamycin prevent neurotoxic effects of anti-cancer drugs on cultured embryonic sensory neurons. Neuropharmacology 40:947–953
96. Xu L, Ouyang YB, Giffard RG (2003) Geldanamycin reduces necrotic and apoptotic injury due to oxygen-glucose deprivation in astrocytes. Neurol Res 25:697–700
97. Ouyang YB, Xu L, Giffard RG (2005) Geldanamycin treatment reduces delayed CA1 damage in mouse hippocampal organotypic cultures subjected to oxygen glucose deprivation. Neurosci Lett 380:229–233
98. Dou F, Yuan LD, Zhu JJ (2005) Heat shock protein 90 indirectly regulates ERK activity by affecting Raf protein metabolism. Acta Biochim Biophys Sin (Shanghai) 37: 501–505
99. Stancato LF, Chow YH, Hutchison KA, Perdew GH, Jove R, Pratt WB (1993) Raf exists in a native heterocomplex with hsp90 and p50 that can be reconstituted in a cell-free system. J Biol Chem 268:21711–21716
100. Ferrer I, Blanco R, Carmona M, Ribera R, Goutan E, Puig B, Rey MJ, Cardozo A, Vinals F, Ribalta T (2001) Phosphorylated map kinase (ERK1, ERK2) expression is associated with early tau deposition in neurones and glial cells, but not with increased nuclear DNA vulnerability and cell death, in Alzheimer disease, Pick's disease, progressive supranuclear palsy and corticobasal degeneration. Brain Pathol 11:144–158
101. Pei JJ, Braak H, An WL, Winblad B, Cowburn RF, Iqbal K, Grundke-Iqbal I (2002) Up-regulation of mitogen-activated protein kinases ERK1/2 and MEK1/2 is associated with the progression of neurofibrillary degeneration in Alzheimer's disease. Brain Res Mol Brain Res 109:45–55
102. LaFevre-Bernt MA, Ellerby LM (2003) Kennedy's disease. Phosphorylation of the polyglutamine-expanded form of androgen receptor regulates its cleavage by caspase-3 and enhances cell death. J Biol Chem 278:34918–34924

103. Murray B, Alessandrini A, Cole AJ, Yee AG, Furshpan EJ (1998) Inhibition of the p44/42 MAP kinase pathway protects hippocampal neurons in a cell-culture model of seizure activity. Proc Natl Acad Sci U S A 95:11975–11980
104. Cheung EC, Slack RS (2004) Emerging role for ERK as a key regulator of neuronal apoptosis. Sci STKE 2004:PE45
105. Subramaniam S, Zirrgiebel U, von Bohlen Und Halbach O, Strelau J, Laliberte C, Kaplan DR, Unsicker K (2004) ERK activation promotes neuronal degeneration predominantly through plasma membrane damage and independently of caspase-3. J Cell Biol 165:357–369
106. Zhu X, Lee HG, Raina AK, Perry G, Smith MA (2002) The role of mitogen-activated protein kinase pathways in Alzheimer's disease. NeuroSignals 11:270–281
107. Kaytor MD, Byam CE, Tousey SK, Stevens SD, Zoghbi HY, Orr HT (2005) A cell-based screen for modulators of ataxin-1 phosphorylation. Hum Mol Genet 14:1095–1105
108. Sato S, Fujita N, Tsuruo T (2000) Modulation of Akt kinase activity by binding to Hsp90. Proc Natl Acad Sci U S A 97:10832–10837
109. George P, Bali P, Cohen P, Tao J, Guo F, Sigua C, Vishvanath A, Fiskus W, Scuto A, Annavarapu S, Moscinski L, Bhalla K (2004) Cotreatment with 17-allylamino-demethoxygeldanamycin and FLT-3 kinase inhibitor PKC412 is highly effective against human acute myelogenous leukemia cells with mutant FLT-3. Cancer Res 64:3645–3652
110. Datta SR, Brunet A, Greenberg ME (1999) Cellular survival: a play in three Akts. Genes Dev 13:2905–2927
111. Pai KS, Cunningham DD (2002) Geldanamycin specifically modulates thrombin-mediated morphological changes in mouse neuroblasts. J Neurochem 80:715–718
112. Xu W, Marcu M, Yuan X, Mimnaugh E, Patterson C, Neckers L (2002) Chaperone-dependent E3 ubiquitin ligase CHIP mediates a degradative pathway for c-ErbB2/Neu. Proc Natl Acad Sci U S A 99:12847–12852
113. Lavictoire SJ, Parolin DA, Klimowicz AC, Kelly JF, Lorimer IA (2003) Interaction of Hsp90 with the nascent form of the mutant epidermal growth factor receptor EGFRvIII. J Biol Chem 278:5292–5299
114. Chen G, Cao P, Goeddel DV (2002) TNF-induced recruitment and activation of the IKK complex require Cdc37 and Hsp90. Mol Cell 9:401–410
115. Luedde T, Assmus U, Wustefeld T, Meyer zu Vilsendorf A, Roskams T, Schmidt-Supprian M, Rajewsky K, Brenner DA, Manns MP, Pasparakis M, Trautwein C (2005) Deletion of IKK2 in hepatocytes does not sensitize these cells to TNF-induced apoptosis but protects from ischemia/reperfusion injury. J Clin Invest 115:849–859
116. Apostol BL, Illes K, Pallos J, Bodai L, Wu J, Strand A, Schweitzer ES, Olson JM, Kazantsev A, Marsh JL, Thompson LM (2006) Mutant huntingtin alters MAPK signaling pathways in PC12 and striatal cells: ERK1/2 protects against mutant huntingtin-associated toxicity. Hum Mol Genet 15:273–285
117. Song C, Perides G, Liu YF (2002) Expression of full-length polyglutamine-expanded Huntingtin disrupts growth factor receptor signaling in rat pheochromocytoma (PC12) cells. J Biol Chem 277:6703–6707
118. Lievens JC, Rival T, Iche M, Chneiweiss H, Birman S (2005) Expanded polyglutamine peptides disrupt EGF receptor signaling and glutamate transporter expression in Drosophila. Hum Mol Genet 14:713–724
119. Levy Y, Gorshtein A (2005) Chaperones and disease. N Engl J Med 353:2821–2822
120. Pearl LH, Prodromou C (2001) Structure, function, and mechanism of the Hsp90 molecular chaperone. Adv Protein Chem 59:157–186

doi:10.1093/brain/awl096 Brain (2006), 129, 1446–1455

Natural history of spinal and bulbar muscular atrophy (SBMA): a study of 223 Japanese patients

Naoki Atsuta,[1] Hirohisa Watanabe,[1] Mizuki Ito,[1] Haruhiko Banno,[1] Keisuke Suzuki,[1] Masahisa Katsuno,[1] Fumiaki Tanaka,[1] Akiko Tamakoshi[2] and Gen Sobue[1]

Departments of [1]Neurology and [2]Preventive Medicine/Biostatistics and Medical Decision Making, Nagoya University Graduate School of Medicine, Nagoya, Japan

Correspondence to: Gen Sobue, MD, Department of Neurology, Nagoya University Graduate School of Medicine, Nagoya 466-8550, Japan
E-mail: sobueg@med.nagoya-u.ac.jp

Spinal and bulbar muscular atrophy (SBMA) is an adult-onset motoneuron disease caused by a CAG-repeat expansion in the androgen receptor (AR) gene and for which no curative therapy exists. However, since recent research may provide opportunities for medical treatment, information concerning the natural history of SBMA would be beneficial in planning future clinical trials. We investigated the natural course of SBMA as assessed by nine activities of daily living (ADL) milestones in 223 Japanese SBMA patients (mean age at data collection = 55.2 years; range = 30–87 years) followed from 1 to 20 years. All the patients were diagnosed by genetic analysis. Hand tremor was an early event that was noticed at a median age of 33 years. Muscular weakness occurred predominantly in the lower limbs, and was noticed at a median age of 44 years, followed by the requirement of a handrail to ascend stairs at 49, dysarthria at 50, dysphagia at 54, use of a cane at 59 and a wheelchair at 61 years. Twenty-one of the patients developed pneumonia at a median age of 62 and 15 of them died at a median age of 65 years. The most common cause of death in these cases was pneumonia and respiratory failure. The ages at onset of each ADL milestone were strongly correlated with the length of CAG repeats in the AR gene. However CAG-repeat length did not correlate with the time intervals between each ADL milestone, suggesting that although the onset age of each ADL milestone depends on the CAG-repeat length in the AR gene, the rate of disease progression does not. The levels of serum testosterone, an important triggering factor for polyglutamine-mediated motoneuron degeneration, were maintained at relatively high levels even at advanced ages. These results provide beneficial information for future clinical therapeutic trials, although further detailed prospective studies are also needed.

Keywords: natural history; motoneuron disease; SBMA; Kennedy disease; ADL milestone

Abbreviations: ADL = activities of daily living; ALT = alanine aminotransferase; AR = androgen receptor; AST = aspartate aminotransferase; CK = creatine kinase; HbA1c = haemoglobin A1c; SBMA = spinal and bulbar muscular atrophy

Received January 11, 2006. Revised March 19, 2006. Accepted March 23, 2006. Advance Access publication April 18, 2006

Introduction

Spinal and bulbar muscular atrophy (SBMA) is a neurodegenerative disorder of motoneurons characterized by proximal limb muscular atrophy, bulbar involvement, marked contraction fasciculation, hand tremor and gynaecomastia (Kennedy et al., 1968; Sobue et al., 1989). SBMA is caused by a CAG-repeat expansion in the first exon of the androgen receptor (AR) gene on the X-chromosome (La Spada et al., 1991). Similar to other triplet repeat diseases, the age at onset of disease has been inversely linked to the size of the CAG-repeat expansions (Andrew et al., 1993; Sasaki et al., 1996; Rosenblatt et al., 2003). For example, an association between the age at onset of limb muscle weakness and the CAG-repeat length has been demonstrated (Doyu et al., 1992; Igarashi et al., 1992; La Spada et al., 1992; Shimada et al., 1995; Sinnreich et al., 2004). Nuclear accumulation of mutant AR with expanded polyglutamines in motoneurons, as well as in other cells, has been shown to be a major pathogenic process (Li et al., 1998a, b; Adachi et al., 2005). However, the progression and prognosis of SBMA has not been assessed in detail, particularly concerning the influence of CAG-repeat size, the decline of the activities of daily living (ADL) with disease progression and the determination of functional

prognosis. Some SBMA studies reported no correlation between the progression of the clinical course and the number of CAG repeats (Lund et al., 2001; Sperfeld et al., 2002), while other studies revealed an age-assessed severity of limb-muscle weakness (Doyu et al., 1992) or only a weak correlation between the decline of ADL and CAG-repeat expansion (La Spada et al., 1992). Since most of the studies performed thus far contained small sample sizes, the influence of CAG-repeat length on the clinical course of SBMA patients remains obscure. In other CAG-repeat diseases such as Huntington's disease, spinocerebellar ataxia type 3 (SCA3) and dentatorubral-pallidoluysian atrophy (DRPLA), an age-assessed residual cell population, a variety of clinical manifestations and MRI-assessed cerebellar volume have been reported to correlate with CAG-repeat length (Koide et al., 1994; Furtado et al., 1996; Penney et al., 1997; Abe et al., 1998). However, it is still not known how CAG-repeat length influences the progression and prognosis of CAG-repeat diseases.

Recent research has suggested therapeutic approaches to SBMA. In a transgenic mouse model expressing the human AR gene with expanded CAG repeats, progressive muscular atrophy and weakness associated with the nuclear accumulation of mutant AR protein was observed. These phenotypes were significantly ameliorated by anti-testosterone therapy (Katsuno et al., 2002, 2003), and the clinical and pathological phenotypes of these mice were markedly improved by the overexpression of heat shock proteins (Adachi et al., 2003; Katsuno et al., 2005). Furthermore, 17-allylamino-17-demethoxygeldanamycin (17-AAG), a potent HSP90 inhibitor, was recently shown to ameliorate motor function deficits and pathological changes in SBMA transgenic mice (Waza et al., 2005). These remarkable therapeutic effects in the transgenic mouse model strongly suggest the possibility of using these approaches in human clinical trials. In order to prepare for such a therapeutic approach, it is important to establish the natural history of clinical symptoms of SBMA based on a large number of patients.

In the present study, we investigated the natural course of SBMA as assessed by 9 ADL milestones in 223 Japanese SBMA patients, and correlated the age of onset of specific milestones during the course of the disease with the CAG-repeat length in the AR gene.

Patients and methods

Patients and clinical evaluations

Our laboratory diagnosed 303 patients as SBMA by genetic analysis between 1992 and 2004. Two-thirds of the patients were followed in Nagoya University Hospital or affiliated hospitals, while the other patients were from other hospitals nationwide. These patients were followed by neurologists from 1 year to >20 years. We reviewed the clinical course of the disease in 223 out of 303 patients. The initial symptoms and onset of nine ADL milestones were assessed to evaluate the clinical course of the disease. The ADL milestones were defined as follows: hand tremor (patient awareness of hand tremor), muscular weakness (initial patient awareness of muscular weakness in any part of the body), requirement of a handrail (patient was unable to ascend stairs without the use of a handrail), dysarthria (patient was unable to articulate properly and had intelligible speech only with repetition), dysphagia (patient choked occasionally at meals), use of a cane (patient used a cane constantly when away from home), use of a wheelchair (patient used a wheelchair when away from home) and development of pneumonia (patient developed pneumonia that required in-hospital care). The age at death and cause of death were also investigated. We assessed the age at which the ADL milestones first occurred and the age at death by direct interview, examination of the patients, family interviews and by reviewing the patient's clinical record. The milestones that could be recognized by family members, such as the use of a cane, the use of a wheelchair or the development of pneumonia, were confirmed by them wherever possible.

All evaluators used similar criteria to assess each milestone. To verify these nine ADL milestones as characteristic landmarks in the progression of SBMA symptoms, two neurologists independently assessed their onset in SBMA patients. The accordance between the evaluators of the age of onset of each ADL milestone was verified in 20 SBMA patients with Pearson's correlation coefficients ranging from 0.95 to 0.99.

The clinical landmarks adopted in the previous studies that showed clinical courses of SBMA, based on the characteristic symptoms, were onset of weakness, difficulty climbing stairs, being wheelchair-bound, tremor, gynaecomastia, fasciculations, premature exhaustion of muscles and chewing, muscle cramps, muscle pain, dysarthria and dysphagia (Doyu et al., 1992; La Spada et al., 1992; Shimada et al., 1995; Sperfeld et al., 2002; Sinnreich et al., 2004). We excluded development of gynaecomastia and fasciculation from the ADL milestones, since more than one-third of the patients were not aware of these symptoms, despite their presence. The appearance of muscle cramp and exhaustion of muscles and chewing were also excluded as their recognition was extremely variable among the patients. Some patients recognized them at a very early phase, while others did so only at later stages or not at all.

We used the modified Rankin scale (van Swieten et al., 1988) for the assessment of clinical disability in daily life and examined the serum levels of creatine kinase (CK), aspartate aminotransferase (AST), alanine aminotransferase (ALT), total cholesterol, total testosterone and haemoglobin A1c (HbA1c) as laboratory markers for disease status. As controls, we used the serum levels of CK, AST, ALT, total cholesterol and HbA1c from health screening data of 62–70 males aged 24–79 years, free from neuromuscular diseases. For serum testosterone levels, we adopted published control data from 1143 Japanese males determined by the same assay method that we used in this study (Iwamoto et al., 2004).

We implemented the ethics guideline for human genome/gene analysis research and the ethics guideline for epidemiological studies endorsed by the Japanese government. Before we interviewed the patients, we obtained written informed consent. In cases where this was not possible, such as deceased patients, we used only existing material without informed consent and strictly protected anonymity. All of the study plans were approved by the ethics committee of Nagoya University Graduate School of Medicine.

Genetic analysis

Genomic DNA was extracted from peripheral blood of the SBMA patients using conventional techniques. PCR amplification of the

CAG repeat in the AR gene was performed using a fluorescein-labelled forward primer (5′-TCCAGAATCTGTTCCAGAGCGT-GC-3′) and a non-labelled reverse primer (5′-TGGCCTCCGCTCAG-GATGTCTTTAAG-3′). Detailed PCR conditions were described previously (Tanaka et al., 1999). Aliquots of PCR products were combined with loading dye and separated by electrophoresis with an autoread sequencer SQ-5500 (Hitachi Electronics Engineering, Tokyo, Japan). The size of the CAG repeat was analysed on Fraglys software version 2.2 (Hitachi) by comparison with co-electrophoresed PCR standards with known repeat sizes. The CAG-repeat size of the PCR standard was determined by direct sequence as described previously (Doyu et al., 1992).

Data analysis

All variables were summarized using descriptive statistics, including median, mean, SD, percentile and percentages. Age at ADL milestone data from a sufficient number of the patients was evaluated by Kaplan–Meier analyses, and log rank test statistics were used to determine whether Kaplan–Meier transition curves differed among subgroups. Relationships between the age at each ADL milestone and the length of CAG repeat of AR gene were analysed using Pearson's correlation coefficient. Correlations between laboratory test value and the age at examination were also analysed using Pearson's correlation coefficient. P-values of <0.05 were considered to be statistically significant. Calculations were performed using the statistical software package Dr SPSS II for Windows (SPSS Japan Inc., Tokyo, Japan).

Results

Clinical and genetic backgrounds of SBMA patients

A total of 223 SBMA patients were included in this study (Table 1). All of the patients were of Japanese nationality. The mean age at the time of data collection was 55.2 6 10.5 years (range = 30–87 years). The mean duration from onset assessed by the patient's initial awareness of muscle weakness was 9.8 6 7.2 years (range = 0–37).

The mean number of CAG repeats in the AR gene was 46.6 6 3.5 (range = 40–57). The location of the initial noticeable muscular weakness was lower extremities in 70.5%, upper extremities in 31.0%, bulbar symptoms in 11.4% and facial weakness in 2.4%. Some patients noticed muscle weakness initially in two locations simultaneously; thus overlap between the groups existed. Weakness in the lower extremities was noticed most often as difficulty in climbing stairs, followed by difficulty in walking for long distances and difficulty in standing from a sitting position. Bulbar symptoms were first noticed as a difficulty in articulating properly. ADL assessed by a modified Rankin scale at examination was 0–1 in 17.2%, 2–3 in 66.1% and 4–6 in 16.7% of the patients. Serum CK levels were 863.5 6 762.5 IU/l (range = 31–4955; normal value = 45–245 IU/l), HbA1c levels were 5.7 6 1.1% (range = 4.3–9.6; normal value = 4.3–5.8%), serum testosterone levels were 6.48 6 1.83 ng/ml (range = 2.85–10.20; normal value = 2.7–10.7 ng/ml), serum AST levels were 44.3 6 29.4 IU/l (range = 17–238; normal value = 0–41 IU/l), serum ALT levels were 52.6 6 37.1 IU/l (range = 12–248; normal value = 0–45 IU/l) and serum total cholesterol levels were 219.3 6 42.3 mg/dl (range = 119–413; normal value = 120–220 mg/dl).

Table 1 Clinical and genetic backgrounds of SBMA patients

Clinical and genetic features	Mean 6 SD (range)
Age at examination (years)	55.2 6 10.5 (30–87)
Duration from onset (years)[a]	9.8 6 7.2 (0–37)
CAG-repeat length in AR gene (number)	46.6 6 3.5 (40–57)
Location of initial muscular weakness the patients perceived (%)[b]	
Facial	2.4
Bulbar	11.4
Upper extremities	31.0
Lower extremities	70.5
Modified Rankin scale at examination (%)	
0–1	17.2
2–3	66.1
4–6	16.7
Serum markers at examination	
Serum CK (n = 182) (IU/l)	863.5 6 762.5 (31–4955)
HbA1c level (n = 76) (%)	5.7 6 1.1 (4.3–9.6)
Serum testosterone level (n = 61) (ng/ml)	6.48 6 1.83 (2.85–10.20)
Serum AST (n = 130) (IU/l)	44.3 6 29.4 (17–238)
Serum ALT (n = 133) (IU/l)	52.6 6 37.1 (12–248)
Total cholesterol level (n = 82) (mg/dl)	219.3 6 42.3 (119–413)

Normal values for serum CK range = 45–245 IU/l; HbA1c range = 4.3–5.8%; serum testosterone range = 2.7–10.7 ng/ml; serum AST range = 0–41 IU/l; serum ALT range = 0–45 IU/l; and total cholesterol range = 120–220 mg/dl. [a]Onset was assessed by patients' initial awareness of muscle weakness; [b]some patients noticed muscle weakness in two locations simultaneously.

Age at which ADL milestones appear

Age distributions at which the ADL milestones initially appeared are summarized in Fig. 1. Hand tremor was the earliest of the ADL milestones that the patients noticed, and it occurred at a median age of 33 years. Hand tremor was particularly noticed when patients used their hands such as in holding a drinking glass. Muscular weakness, predominantly in the lower extremities, was noticed at a median age of 44 years, followed by the need of a handrail when going up stairs at a median age of 49 years. Dysarthria, dysphagia and the use of a cane appeared at median ages of 50, 54 and 59 years, respectively. The use of a wheelchair started at a median age of 61 years. Patients developed pneumonia owing to aspiration and required in-hospital care at a median age of 62 years. The median age of those 15 patients who died before this report was 65 years. The predominant cause of death in eight of these cases was aspiration pneumonia. One patient died of lung cancer, and another patient died from ischaemic heart disease. One patient committed suicide. The causes of death of the other four patients were unknown. The ages of

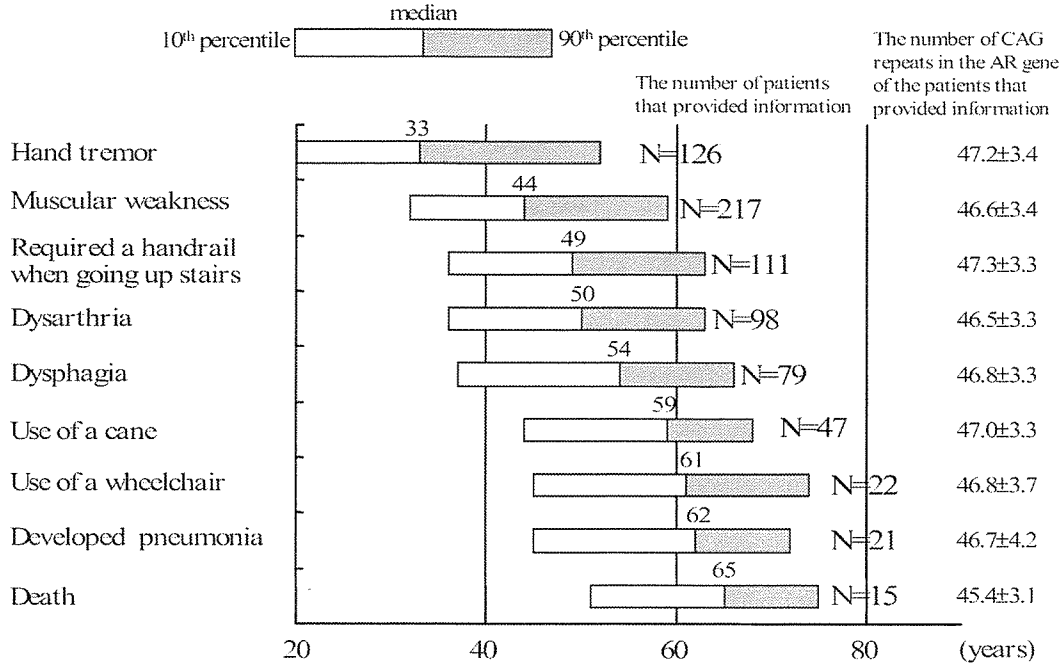

Fig. 1 Age distribution of ADL milestones for 223 SBMA patients. The mean number of CAG repeats in the AR gene of the patients does not differ significantly as shown at the right.

onset of each ADL milestone showed a considerable wide-ranged distribution from 25 to 30 years when assessed from the 10th to 90th percentile range. Although there were no significant differences in the mean number of CAG repeats in the AR gene of the patients in which we assessed the age at onset of each ADL milestone (Fig. 1), suggesting that age distributions at each milestone were derived from genetically uniform patients, we tested the hypothesis that the wide range in ages of onset at each milestone may be due to individual differences in CAG-repeat lengths.

Age at onset of each ADL milestone correlates well with CAG-repeat length

As shown in Fig. 2, the onset age of the individual ADL milestones examined showed significant correlations with the CAG-repeat length of the patients reporting on these symptoms ($r = -0.853$ to -0.447, $P < 0.016$–0.001). Of these, age at onset of hand tremor, requirement of a handrail, use of a wheelchair, developing pneumonia requiring in-hospital care and death were strongly correlated with the CAG repeats with $r < -0.5$. Furthermore, the onset ages of pneumonia and death were highly correlated with the CAG repeats with $r = -0.78$ and -0.85, respectively, indicating that these specific events, the onset ages of which the patients or their families were able to indicate more definitely, showed a more significant correlation with the CAG-repeat length than other ADL milestones.

Since 47 repeats was the median CAG-repeat length of the entire patient group, we further compared the Kaplan–Meier curves for age at onset of hand tremor, muscular weakness and requirement of a handrail between the patient group with 47 CAG repeats or more and those with <47 CAG repeats (Fig. 3). We assessed only these three ADL milestones, since the number of patients in these groups was sufficient to perform a log rank test analysis. The patients with <47 CAG repeats showed regression curves shifted by ~10 years compared with those with ≥47 CAG repeats (Fig. 3, $P < 0.001$ in log rank test). Together, these observations strongly suggest that the onset age of each ADL milestone is highly dependent on CAG-repeat length in the AR gene.

CAG-repeat length does not correlate with the rate of disease progression assessed by ADL milestones

In order to assess whether CAG-repeat length influences the disease progression rate, we examined the relationship between the time intervals from onset age of muscular weakness to that of requirement of a handrail when going up stairs, use of a cane, use of a wheelchair, development of pneumonia and death and the CAG-repeat lengths in these groups (Fig. 4). We did not find any significant correlations of the intervals among the onset age of the various milestones with the CAG-repeat length, suggesting that the progression rate of the disease is not significantly influenced by the CAG-repeat size.

In addition, we examined the declining regression assessed by those ADL milestones in individual patients with ≥47 CAG repeats compared with those with <47 (Fig. 5). These regression lines were divergent from each other, possibly because of divergent CAG-repeat size, while the mean slopes

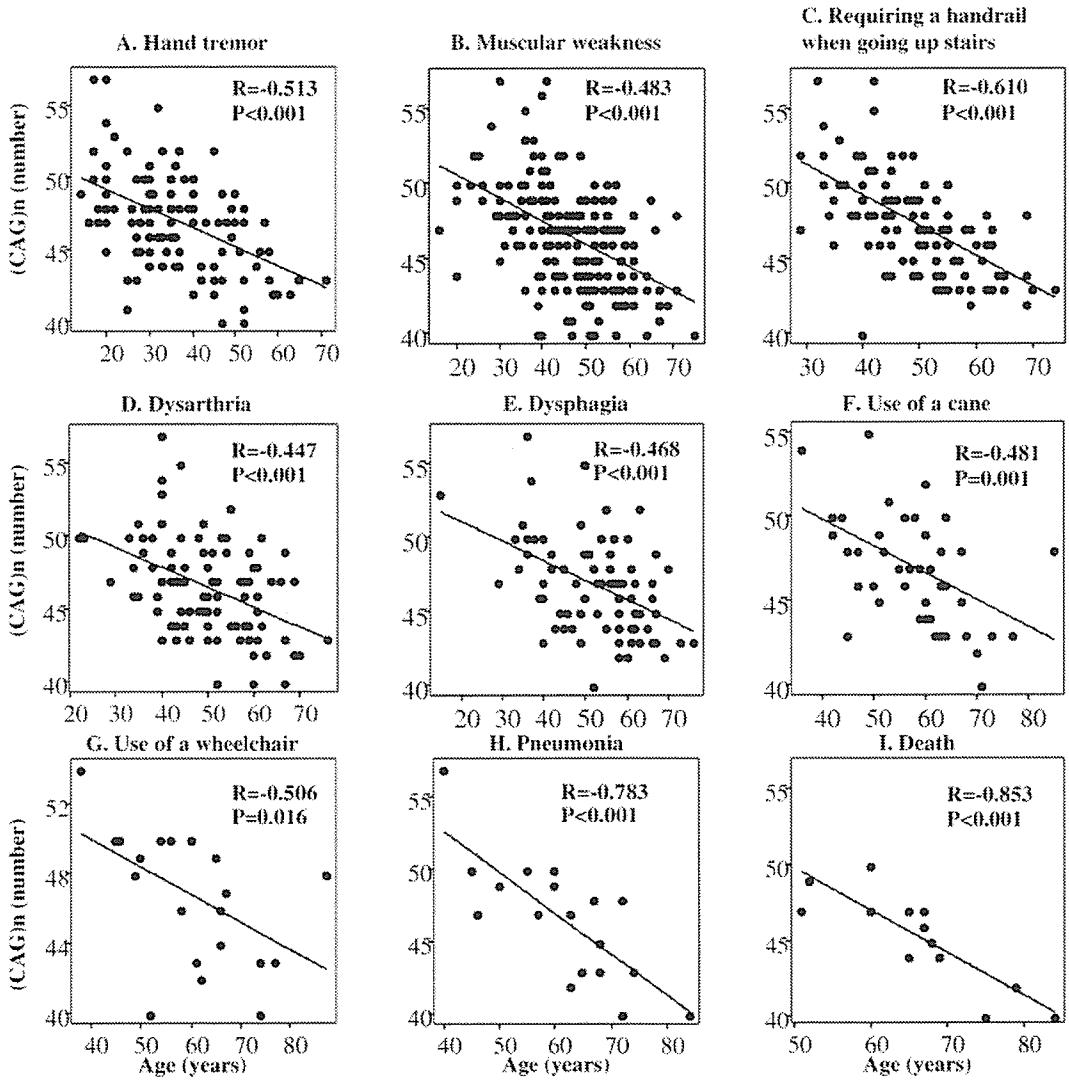

Fig. 2 (A–I) Correlation of the CAG-repeat number of and the age at each ADL milestone. There were significant correlations between CAG number and age at all milestones analysed using Pearson's correlation coefficient.

of the regression lines of the two groups were likely to be parallel. There were no significant differences between the interval times of the two groups as assessed by unpaired t-test (Fig. 5), suggesting, again, that the rate of disease progression was not markedly dependent upon the size of the CAG repeats.

Age-related changes of laboratory data and their relation to CAG repeats

Glucose intolerance, serum CK and ALT elevation and androgen insensitivity of SBMA patients have been reported (Sobue et al., 1989; Shimada et al., 1995; Dejager et al., 2002; Sinnreich et al., 2004). We examined the relationship between serum CK, HbA1c, testosterone, total cholesterol, AST and ALT levels and the age and CAG-repeat length of the patients. The serum levels of CK, AST and ALT were elevated in subpopulations of patients, particularly in the early phase of the disease, while these levels gradually declined with age (Fig. 6A, E and F). In advanced ages, the levels of these serum markers had declined to nearly normal levels. Serum testosterone levels were slightly elevated from control values in one-third of patients; in general, they declined slightly with age (Fig. 6C). However, even at these advanced ages testosterone levels were within or above the normal range. In contrast, HbA1c levels were within the normal range in the patients with short disease durations, but they gradually increased to above the normal range as the age of patients increased (Fig. 6B). Cholesterol levels were mildly elevated in some patients, but there was no particular age-dependent change observed (Fig. 6D). Elevated levels of these serum markers were not correlated with the CAG-repeat sizes (data not shown). Therefore, the levels of these markers appear to reflect the active pathological process of the disease, especially in the early or late phases, but their significance should be examined further.

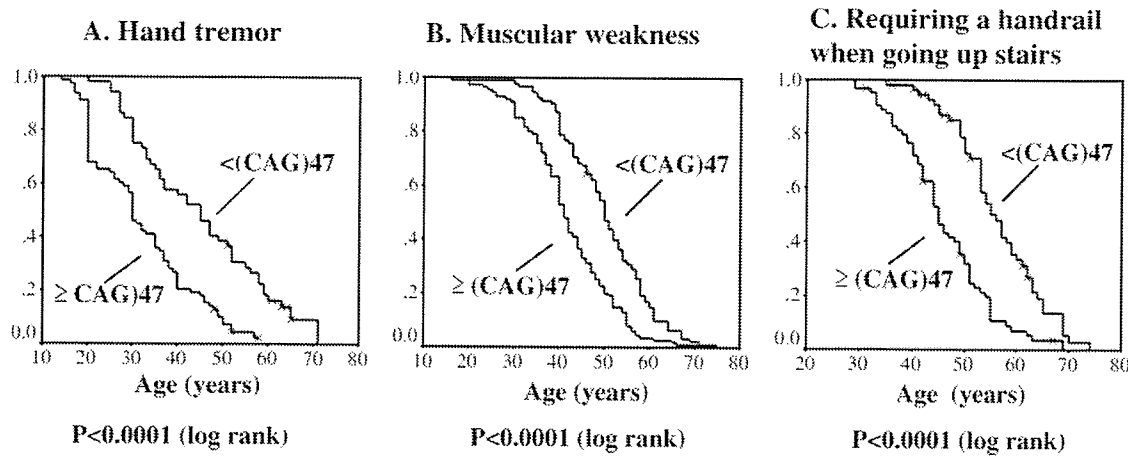

Fig. 3 (A–C) Kaplan–Meier analysis of age at onset of hand tremor, muscular weakness and requirement of a handrail. There was a highly significant difference between the patient group with ≥47 CAG repeats and the group with <47 CAG repeats, as compared by log rank tests.

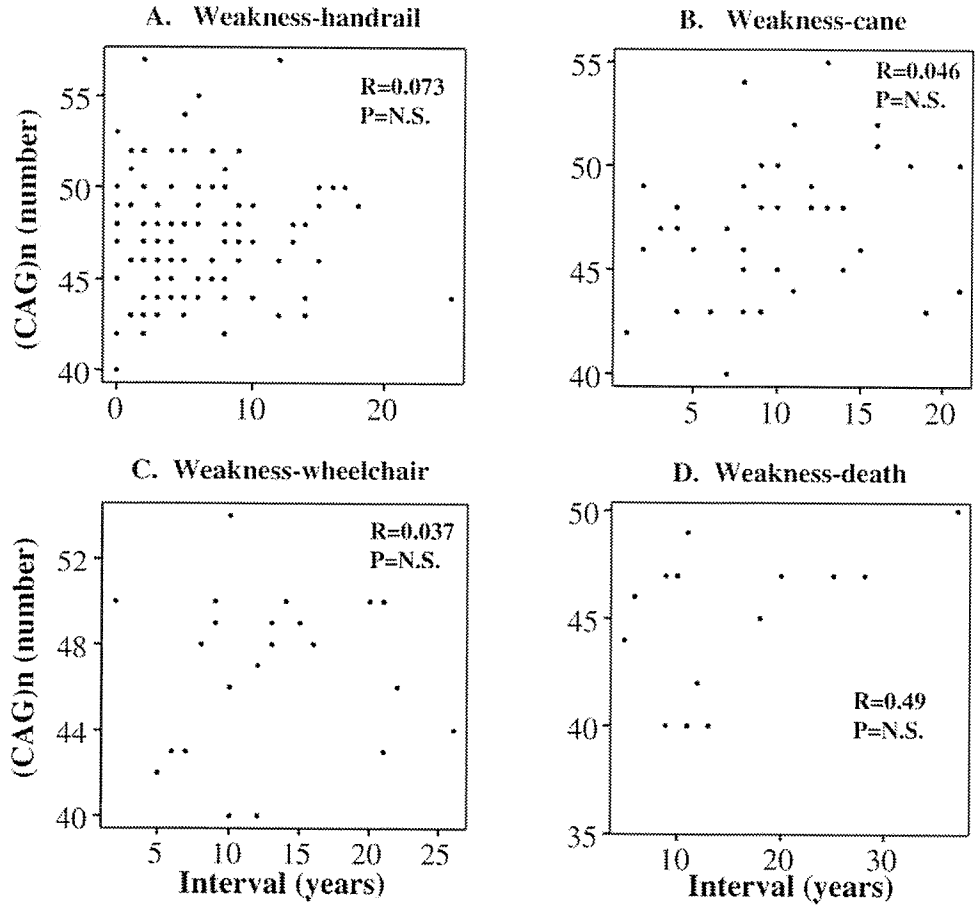

Fig. 4 (A–D) Correlation between the AR gene CAG number and the time interval between the ADL milestones. The time interval from the age at first awareness of muscular weakness to the age at requirement of a handrail, use of a cane, use of a wheelchair and death were compared with the CAG number by Pearson's correlation coefficient. There were no significant correlations in any of the interval times.

Discussion

Our study elucidated the natural history of SBMA patients based on nine ADL milestones. SBMA progressed slowly to the end stage with a median duration from onset assessed by muscle weakness to the appearance of pneumonia of 16 years, and to death of 22 years whereas the median durations from age of onset to the age of requirement of a handrail, dysarthria and dysphagia were 5, 6 and 10 years, respectively,

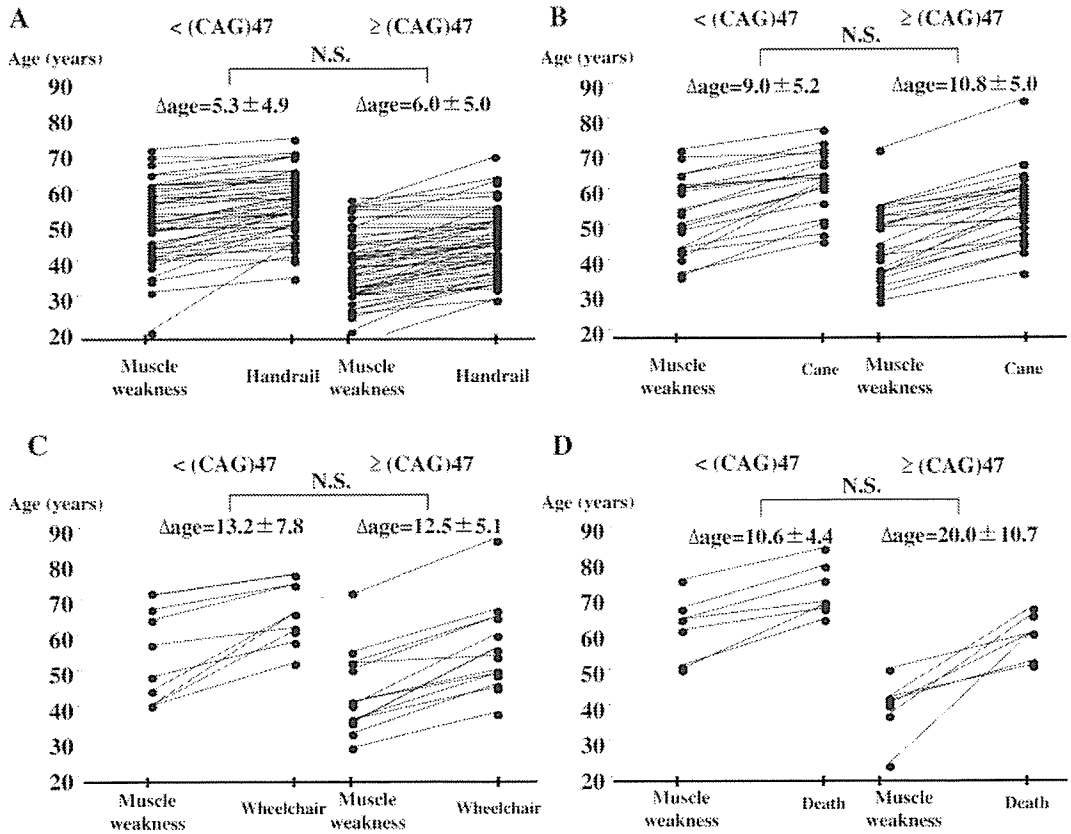

Fig. 5 (A–D) Individual case presentation of the declining regression assessed by ADL milestones. The interval times from the age at first awareness of weakness to the age at requirement of a handrail, use of a cane, use of a wheelchair and death are described for individual patients from two groups, those with <47 CAG repeats and those with ≥47 repeats. These regression lines were divergent from each other, possibly owing to divergent CAG-repeat size, while the mean slopes of the regression lines were likely to be parallel among the two subgroups of patients. There were no significant differences between the interval times of the two groups of patients analysed by unpaired t-test.

indicating that the ADL deterioration leading to a decline in the quality of daily living during early phases of the diseases is significant, in spite of a relatively long lifespan. The lifespan of SBMA patients was previously speculated to be 10–15 years shorter than those of the general Japanese male population (Mukai, 1989). In this study, 15 of the 223 patients died at a median age of 65 years. Although there are too few data to make a reliable calculation, this is ~12 years shorter than that of the current lifespan of the normal Japanese male indicated by the abridged life table announced by the Japanese Ministry of Health, Labor and Welfare in 2003, and, thus, is consistent with the previous speculation (Mukai, 1989). Of these 15 patients, the most common cause of death was pneumonia due to aspiration and dysphagia. Thus, the bulbar symptoms, such as difficulty in proper articulation and mild dysphagia, were relatively mild in their early manifestations, but were serious symptoms in the late phase of the disease, when the patients were prone to death. The progression was apparently slower than that of ALS, another adult-onset motoneuron disease, which occasionally mimics SBMA phenotypes, particularly in the early phase (La Spada et al., 1992; Parboosingh et al., 1997; Traynor et al., 2000).

The onset ages of each ADL milestone were extremely variable, but all were well correlated with the CAG-repeat size in the AR gene. Patients with longer CAG-repeat sizes showed an earlier onset age of each ADL milestone examined, including occurrence of pneumonia or death in the end stage. Several previous studies also documented the natural history of SBMA. They showed that the age of disease onset assessed by muscle weakness was strongly correlated with AR gene CAG-repeat size (Doyu et al., 1992; Igarashi et al., 1992; La Spada et al., 1992; Shimada et al., 1995), whereas the onset ages of other symptoms such as fatigue, tremor, occurrence of gynaecomastia and severity of muscle weakness were not significantly correlated with repeat size (La Spada et al., 1992; Amato et al., 1993; Mariotti et al., 2000; Dejager et al., 2002; Sperfeld et al., 2002). It is not clear why the relations between the onset age of these symptoms and CAG repeat size were not apparent in these reports, since significant correlations with the onset age of hand tremor and muscular weakness were confirmed in the present study. One possibility may be the relatively small sample sizes in the previous studies (Amato et al., 1993; Sperfeld et al., 2002). An alternative explanation may be that very early symptoms, such as

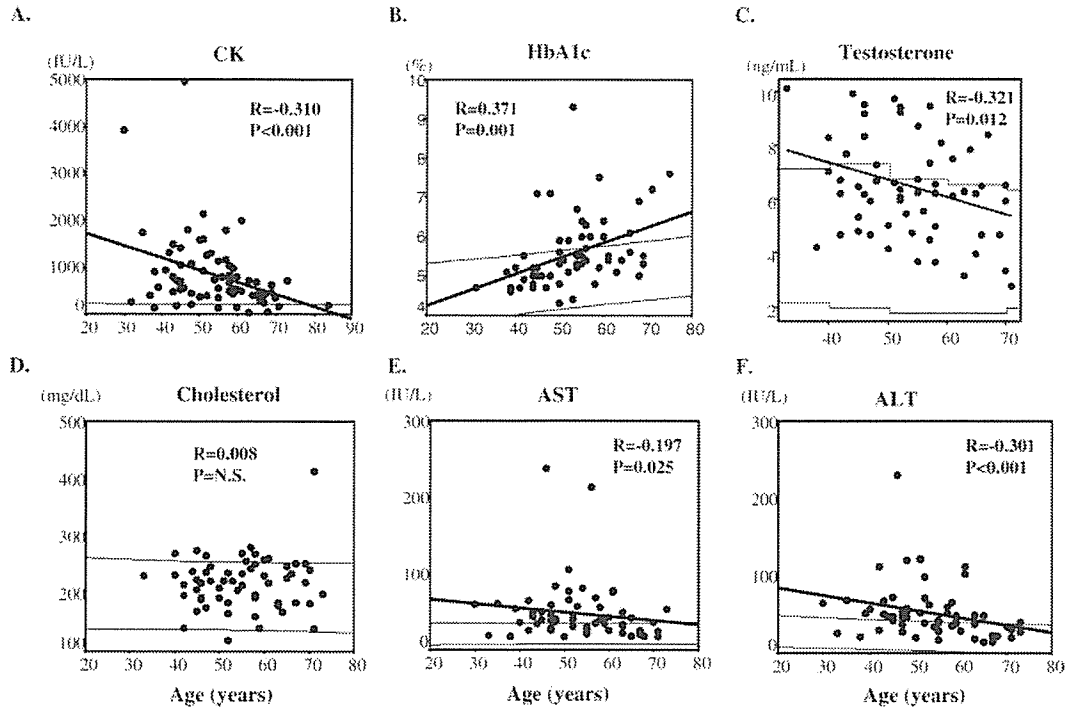

Fig. 6 (A–F) Correlation between the levels of serum markers and the age at examination. A weak, but significant, correlation was seen between HbA1c and age, while weak, but significant, inverse correlations were seen between CK, testosterone, AST and ALT and age as analysed by Pearson's correlation coefficient. Cholesterol levels were not correlated with age. The thin lines in each plot indicate the 95% confidence intervals calculated from control subjects.

gynaecomastia and fatigue, are not very accurate or reliable markers for ADL milestones compared with later symptoms, especially in a retrospective study. Indeed, the correlation of the onset age of tremor with CAG-repeat size was weaker than that of the onset age of the use of a wheelchair or a cane, which were more advanced ADL milestones used in our study.

The relationship between CAG-repeat size, disease markers and rate of disease progression have also been assessed extensively in Huntington's disease (Illarioshkin et al., 1994; Brandt et al., 1996; Furtado et al., 1996; Penney et al., 1997; Rosenblatt et al., 2003). Neuronal loss in the caudate nucleus and putamen, adjusted for age of death, correlated well with CAG-repeat length (Furtado et al., 1996; Penney et al., 1997; Rosenblatt et al., 2003). The rate of progression assessed by symptom severity controlled by duration from onset (Illarioshkin et al., 1994) also correlated strongly with the CAG-repeat size. In addition, we previously demonstrated that the extent of cerebellar atrophy and severity of muscle weakness, both adjusted by age at examination correlated well with CAG-repeat size in SCA3 and SBMA, respectively (Doyu et al., 1992; Abe et al., 1998). These observations suggested that longer CAG repeats resulted in an earlier age at onset and greater neuronal loss when compared with shorter repeats. There is also some evidence that they contribute to a faster rate of clinical decline.

In our present study, as documented in Figs 2 and 3, patients with longer CAG repeats reached each of the ADL milestones such as hand tremor, muscle weakness or the requirement of a handrail when going up stairs much earlier than did the patients with shorter CAG repeats. Interestingly, however, the decline curves, as documented with Kaplan–Meier analyses, for these individual milestones were similar (Fig. 3), with an ~10-year difference between the patients with ≥47 repeats and those with <47 repeats. The earlier age at onset for each ADL milestone in patients with longer repeat lengths is similar to observations in cases of Huntington's disease.

The most striking observation in our study was that the interval periods between individual ADL milestones, such as between onset of muscle weakness and that of requirement of a handrail, use of a cane, being wheelchair-bound or death were not affected by the CAG-repeat length (Figs 4 and 5). Although patients with longer CAG-repeat size reached individual ADL milestones faster than those with shorter repeats, the decline rate from one ADL milestone to another was not influenced by the CAG-repeat size. These results suggest that the rate of disease progression assessed by ADL milestones is not influenced by CAG-repeat length.

Therefore, we may propose a view simulating the natural history of SBMA, in that, the decline curves of ADL in the SBMA patients with longer CAG-repeat size are shifted earlier than those in the SBMA patients with shorter CAG-repeat size, and the slopes of the decline curves are parallel to one another.

The phenotypic decline curves provided by mouse models of CAG-repeat diseases (Adachi et al., 2003; von Horsten et al., 2003) also support our view of the natural history of SBMA. The present findings are informative in understanding the pathophysiology of SBMA. CAG-repeat size is known to be a determinant factor for the entry of neuronal cells harbouring a mutant AR gene with expanded CAG repeats into the neuronal degeneration process in vitro, as well as in vivo (Mangiarini et al., 1996). However, it is not known whether the rate of neuronal degeneration leading to subsequent cell death is dependent on CAG-repeat size. Once neuronal cell degeneration or neuronal cell dysfunction is initiated, the progression of degeneration to cell death may be determined by intrinsic factors such as a cell death processing system other than the CAG-repeat size. Thus, we suggest that the onset time of certain ADL milestones reflects how many neurons have entered into the neurodegeneration-dysfunction process, which is determined by CAG-repeat size, rather than the intrinsic cell death process.

Recently, we demonstrated that several interventions, anti-testosterone therapy with leuprorelin (Katsuno et al., 2003), induction of Hsp70 (Adachi et al., 2003; Katsuno et al., 2005), inhibition of HDAC (Minamiyama et al., 2004) or inhibition of Hsp90 (Waza et al., 2005) showed potent therapeutic effects in improving the characteristic phenotypes and pathology in the SBMA transgenic mouse model. These observations strongly encourage the application of the therapeutics to human SBMA patients. Unlike the therapeutic approach commonly taken in neurodegenerative diseases of replacing lost substances such as neurotransmitters, these new therapeutics ameliorate the disease progression itself by preventing pathological molecular processes. Since the progression of SBMA is slow, clinical end-points will be useful for efficiently assessing the effectiveness of these therapies. The present study may indicate ADL milestones that can be clinical end-points in therapeutic trials. However, assessing the ADL milestones adopted in this study, such as the use of a cane or a wheelchair, would take years during clinical trials. Thus, we need to find a shorter-term surrogate marker that reflects the pathological process, although a genuine clinical therapeutic end-point should be examined to determine whether the ADL milestones are effectively delayed by the therapeutic intervention.

One interesting observation in this study is that serum testosterone levels were maintained at relatively high levels, even at advanced ages, although they did decrease with age (Fig. 6C). Since testosterone is an important triggering factor for polyglutamine-mediated motoneuron degeneration (Katsuno et al., 2002, 2003), these findings suggest that anti-testosterone therapy with leuprorelin (Katsuno et al., 2003) may be applicable even in aged SBMA patients.

The advantages of our study over previous studies are the large sample size and the employment of marked and apparent ADL milestones that the patients recognized easily. Nevertheless, several limitations are also present. One major limitation is that the study was retrospective in design and the decline curve was not successively and prospectively assessed in individual patients. A prospective study that follows individual patients in assessing the ADL milestones is needed to ascertain the validity of this natural history of SBMA.

The ADL milestones that we adopted for this study were selected with the assumption that they could be accurately assessed by us, the patients or family members, even in a retrospective study. However, as we demonstrated, the development of pneumonia and death showed higher significant correlations with CAG-repeat size than did other earlier ADL milestones such as the appearance of hand tremor or dysarthria, suggesting that these critical end-stage events may be more accurately assessed in a retrospective manner. We need further long-standing prospective studies to assess the disease progression more properly.

Acknowledgements

This study was supported by a COE grant from the Ministry of Education, Science and Sports of Japan and grants from the Ministry of Welfare, Health and Labor of Japan.

References

Abe Y, Tanaka F, Matsumoto M, Doyu M, Hirayama M, Kachi T, et al. CAG repeat number correlates with the rate of brainstem and cerebellar atrophy in Machado-Joseph disease. Neurology 1998; 51: 882–4.

Adachi H, Katsuno M, Minamiyama M, Sang C, Pagoulatos G, Angelidis C, et al. Heat shock protein 70 chaperone overexpression ameliorates phenotypes of the spinal and bulbar muscular atrophy transgenic mouse model by reducing nuclear-localized mutant androgen receptor protein. J Neurosci 2003; 23: 2203–11.

Adachi H, Katsuno M, Minamiyama M, Waza M, Sang C, Nakagomi Y, et al. Widespread nuclear and cytoplasmic accumulation of mutant androgen receptor in SBMA patients. Brain 2005; 128: 659–70.

Amato AA, Prior TW, Barohn RJ, Snyder P, Papp A, Mendell JR. Kennedy's disease: a clinicopathologic correlation with mutations in the androgen receptor gene. Neurology 1993; 43: 791–4.

Andrew SE, Goldberg YP, Kremer B, Telenius H, Theilmann J, Adam S, et al. The relationship between trinucleotide (CAG) repeat length and clinical features of Huntington's disease. Nat Genet 1993; 4: 398–403.

Brandt J, Bylsma FW, Gross R, Stine OC, Ranen N, Ross CA. Trinucleotide repeat length and clinical progression in Huntington's disease. Neurology 1996; 46: 527–31.

Dejager S, Bry-Gauillard H, Bruckert E, Eymard B, Salachas F, LeGuern E, et al. A comprehensive endocrine description of Kennedy's disease revealing androgen insensitivity linked to CAG repeat length. J Clin Endocrinol Metab 2002; 87: 3893–901.

Doyu M, Sobue G, Mukai E, Kachi T, Yasuda T, Mitsuma T, et al. Severity of X-linked recessive bulbospinal neuronopathy correlates with size of the tandem CAG repeat in androgen receptor gene. Ann Neurol 1992; 32: 707–10.

Furtado S, Suchowersky O, Rewcastle B, Graham L, Klimek ML, Garber A. Relationship between trinucleotide repeats and neuropathological changes in Huntington's disease. Ann Neurol 1996; 39: 132–6.

Igarashi S, Tanno Y, Onodera O, Yamazaki M, Sato S, Ishikawa A, et al. Strong correlation between the number of CAG repeats in androgen receptor genes and the clinical onset of features of spinal and bulbar muscular atrophy. Neurology 1992; 42: 2300–2.

Illarioshkin SN, Igarashi S, Onodera O, Markova ED, Nikolskaya NN, Tanaka H, et al. Trinucleotide repeat length and rate of progression of Huntington's disease. Ann Neurol 1994; 36: 630–5.

Iwamoto T, Yanase T, Koh E, Horie H, Baba K, Namiki M, et al. Reference ranges of serum total and free testosterone in Japanese male adults. Nihon Hinyoukigakkai Zassi (in Japanese) 2004; 95: 751–60.

Katsuno M, Adachi H, Kume A, Li M, Nakagomi Y, Niwa H, et al. Testosterone reduction prevents phenotypic expression in a transgenic mouse model of spinal and bulbar muscular atrophy. Neuron 2002; 35: 843–54.

Katsuno M, Adachi H, Doyu M, Minamiyama M, Sang C, Kobayashi Y, et al. Leuprorelin rescues polyglutamine-dependent phenotypes in a transgenic mouse model of spinal and bulbar muscular atrophy. Nat Med 2003; 9: 768–73.

Katsuno M, Sang C, Adachi H, Minamiyama M, Waza M, Tanaka F, et al. Pharmacological induction of heat-shock proteins alleviates polyglutamine-mediated motor neuron disease. Proc Natl Acad Sci USA 2005; 102: 16801–6.

Kennedy WR, Alter M, Sung JH. Progressive proximal spinal and bulbar muscular atrophy of late onset. A sex-linked recessive trait. Neurology 1968; 18: 671–80.

Koide R, Ikeuchi T, Onodera O, Tanaka H, Igarashi S, Endo K, et al. Unstable expansion of CAG repeat in hereditary dentatorubral-pallidoluysian atrophy (DRPLA). Nat Genet 1994; 6: 9–13.

La Spada AR, Wilson EM, Lubahn DB, Harding AE, Fischbeck KH. Androgen receptor gene mutations in X-linked spinal and bulbar muscular atrophy. Nature 1991; 352: 77–9.

La Spada AR, Roling DB, Harding AE, Warner CL, Spiegel R, Hausmanowa-Petrusewicz I, et al. Meiotic stability and genotype-phenotype correlation of the trinucleotide repeat in X-linked spinal and bulbar muscular atrophy. Nat Genet 1992; 2: 301–4.

Li M, Miwa S, Kobayashi Y, Merry DE, Yamamoto M, Tanaka F, et al. Nuclear inclusions of the androgen receptor protein in spinal and bulbar muscular atrophy. Ann Neurol 1998a; 44: 249–54.

Li M, Nakagomi Y, Kobayashi Y, Merry DE, Tanaka F, Doyu M, et al. Nonneural nuclear inclusions of androgen receptor protein in spinal and bulbar muscular atrophy. Am J Pathol 1998b; 153: 695–701.

Lund A, Udd B, Juvonen V, Andersen PM, Cederquist K, Davis M, et al. Multiple founder effects in spinal and bulbar muscular atrophy (SBMA, Kennedy disease) around the world. Eur J Hum Genet 2001; 9: 431–6.

Mangiarini L, Sathasivam K, Seller M, Cozens B, Harper A, Hetherington C, et al. Exon 1 of the HD gene with an expanded CAG repeat is sufficient to cause a progressive neurological phenotype in transgenic mice. Cell 1996; 87: 493–506.

Mariotti C, Castellotti B, Pareyson D, Testa D, Eoli M, Antozzi C, et al. Phenotypic manifestations associated with CAG-repeat expansion in the androgen receptor gene in male patients and heterozygous females: a clinical and molecular study of 30 families. Neuromuscul Disord 2000; 10: 391–7.

Minamiyama M, Katsuno M, Adachi H, Waza M, Sang C, Kobayashi Y, et al. Sodium butyrate ameliorates phenotypic expression in a transgenic mouse model of spinal and bulbar muscular atrophy. Hum Mol Genet 2004; 13: 1183–92.

Mukai E. Clinical features of bulbo-spinal muscular atrophy. Shinkeinaika (in Japanese) 1989; 30: 1–7.

Parboosingh JS, Figlewicz DA, Krizus A, Meininger V, Azad NA, Newman DS, et al. Spinobulbar muscular atrophy can mimic ALS: the importance of genetic testing in male patients with atypical ALS. Neurology 1997; 49: 568–72.

Penney JB Jr, Vonsattel JP, MacDonald ME, Gusella JF, Myers RH. CAG repeat number governs the development rate of pathology in Huntington's disease. Ann Neurol 1997; 41: 689–92.

Rosenblatt A, Abbott MH, Gourley LM, Troncoso JC, Margolis RL, Brandt J, et al. Predictors of neuropathological severity in 100 patients with Huntington's disease. Ann Neurol 2003; 54: 488–93.

Sasaki H, Fukazawa T, Yanagihara T, Hamada T, Shima K, Matsumoto A, et al. Clinical features and natural history of spinocerebellar ataxia type 1. Acta Neurol Scand 1996; 93: 64–71.

Shimada N, Sobue G, Doyu M, Yamamoto K, Yasuda T, Mukai E, et al. X-linked recessive bulbospinal neuronopathy: clinical phenotypes and CAG repeat size in androgen receptor gene. Muscle Nerve 1995; 18: 1378–84.

Sinnreich M, Sorenson EJ, Klein CJ. Neurologic course, endocrine dysfunction and triplet repeat size in spinal bulbar muscular atrophy. Can J Neurol Sci 2004; 31: 378–82.

Sobue G, Hashizume Y, Mukai E, Hirayama M, Mitsuma T, Takahashi A. X-linked recessive bulbospinal neuronopathy. A clinicopathological study. Brain 1989; 112: 209–32.

Sperfeld AD, Karitzky J, Brummer D, Schreiber H, Haussler J, Ludolph AC, et al. X-linked bulbospinal neuronopathy: Kennedy disease. Arch Neurol 2002; 59: 1921–6.

Tanaka F, Reeves MF, Ito Y, Matsumoto M, Li M, Miwa S, et al. Tissue-specific somatic mosaicism in spinal and bulbar muscular atrophy is dependent on CAG-repeat length and androgen receptor-gene expression level. Am J Hum Genet 1999; 65: 966–73.

Traynor BJ, Codd MB, Corr B, Forde C, Frost E, Hardiman O. Amyotrophic lateral sclerosis mimic syndromes: a population-based study. Arch Neurol 2000; 57: 109–13.

van Swieten JC, Koudstaal PJ, Visser MC, Schouten HJ, van Gijn J. Interobserver agreement for the assessment of handicap in stroke patients. Stroke 1988; 19: 604–7.

von Horsten S, Schmitt I, Nguyen HP, Holzmann C, Schmidt T, Walther T, et al. Transgenic rat model of Huntington's disease. Hum Mol Genet 2003; 12: 617–24.

Waza M, Adachi H, Katsuno M, Minamiyama M, Sang C, Tanaka F, et al. 17-AAG, an Hsp90 inhibitor, ameliorates polyglutamine-mediated motor neuron degeneration. Nat Med 2005; 11: 1088–95.

Available online at www.sciencedirect.com
SCIENCE DIRECT
ELSEVIER
Biochemical and Biophysical Research Communications 343 (2006) 719–730
BBRC
www.elsevier.com/locate/ybbrc

Alteration of familial ALS-linked mutant SOD1 solubility with disease progression: Its modulation by the proteasome and Hsp70

Shingo Koyama [a], Shigeki Arawaka [a,*], Ren Chang-Hong [a], Manabu Wada [a], Toru Kawanami [a], Keiji Kurita [a], Masaaki Kato [b], Makiko Nagai [b], Masashi Aoki [b], Yasuto Itoyama [b], Gen Sobue [c], Pak H. Chan [d], Takeo Kato [a]

[a] Department of Neurology, Hematology, Metabolism, Endocrinology and Diabetology, Yamagata University School of Medicine, 2-2-2 Iida-nishi, Yamagata 990-9585, Japan
[b] Department of Neurology, Tohoku University Graduate School of Medicine, Sendai, Japan
[c] Department of Neurology, Nagoya University Graduate School of Medicine, Nagoya, Japan
[d] Department of Neurosurgery, Stanford University School of Medicine, Stanford, CA, USA

Received 9 February 2006
Available online 9 March 2006

Abstract

Accumulation of misfolded Cu/Zn superoxide dismutase (SOD1) occurs in patients with a subgroup of familial amyotrophic lateral sclerosis (fALS). To identify the conversion of SOD1 from a normally soluble form to insoluble aggregates, we investigated the change of SOD1 solubility with aging in fALS-linked H46R SOD1 transgenic mice. Mutant SOD1 specifically altered to insoluble forms, which were sequentially separated into Triton X-100-insoluble/sodium dodecyl sulfate (SDS)-soluble and SDS-insoluble/formic acid-soluble species. In spinal cords, the levels of SDS-dissociable soluble SOD1 monomers and SDS-stable soluble dimers were significantly elevated before motor dysfunction onset. In COS-7 cells expressing H46R SOD1, treatment with proteasome inhibitors recapitulated the alteration of SOD1 solubility in transgenic mice. In contrast, overexpression of Hsp70 reduced accumulation of mutant-specific insoluble SOD1. SDS-soluble low molecular weight species of H46R SOD1 may appear as early misfolded intermediates when their concentration exceeds the capacity of the proteasome and molecular chaperones.

Keywords: Amyotrophic lateral sclerosis; Cu/Zn superoxide dismutase; Heat shock protein; Proteasome; Oligomer

Amyotrophic lateral sclerosis (ALS) is a neurodegenerative disorder characterized by the degeneration of both upper and lower motor neurons, leading to progressive paralysis. Of all ALS cases, ~90% are sporadic and ~10% are familial; ~20% of familial ALS (fALS) cases are associated with dominantly inherited mutations in the gene encoding Cu/Zn superoxide dismutase (SOD1) [1–3]. SOD1 is a major antioxidant enzyme located predominantly in the cytosol, nucleus, and mitochondrial intermembrane space of eukaryotic cells [4]. The biological active enzyme forms a 32-kDa homodimer and contains one copper-binding site and one zinc-binding site, as well as a disulfide bond in each of its two subunits. SOD1-linked fALS was initially suspected to result from oxidative damage caused by diminished SOD1 activity, but SOD1-null mice show no motor neuron disease [5], and transgenic mice overexpressing human mutant SOD1 have a phenotype that is closely similar to patients with fALS, irrespective of their normal or elevated levels of SOD1 activity [6–9]. This evidence indicates that SOD1-linked fALS occurs due to a toxic gain-of-function of mutant SOD1 but not due to a lowering of its activity [6].

Deposition of proteinaceous inclusions of SOD1 in motor neurons is a characteristic hallmark of patients with fALS [10–12]. Cellular and animal models have shown that overexpression of mutant SOD1 can cause loss of motor

* Corresponding author. Fax: +81 23 628 5318.
E-mail address: arawaka@med.id.yamagata-u.ac.jp (S. Arawaka).

0006-291X/$ - see front matter © 2006 Elsevier Inc. All rights reserved.
doi:10.1016/j.bbrc.2006.02.170

neurons with the formation of SOD1-positive inclusions [12–15] and high-molecular-weight (HMW) SOD1 complexes [12,16–19], supporting the hypothesis that the abnormal accumulation of SOD1 aggregates may play a role in the pathogenesis of fALS. Concerning the formation of SOD1 aggregates, several reports have described a close association with the proteasome and heat shock proteins (Hsps). In cells overexpressing mutant SOD1, inhibition of the proteasome activity resulted in the accumulation of insoluble SOD1 protein and the formation of HMW insoluble complexes [16,17,19–22]. On the other hand, Bruening et al. [23] reported that overexpression of Hsp70 reduced aggregate formation and prolonged cellular viability in cells expressing mutant SOD1. These data imply that the conversion of SOD1 from an inherently soluble form to an aggregated species is promoted by insufficiency of the proteasome and/or molecular chaperones, which suppress the accumulation of misfolded proteins. However, the formation of protein aggregation is a complex process, which contains several kinds of misfolded intermediates to form amorphous aggregates and fibrils [24]. There is only a little basic information on how mutant SOD1 undergoes the complex process in relation to the system of proteasome and Hsps.

In the present study, we investigated the alteration of SOD1 solubility with aging in fALS-linked mutant H46R SOD1 transgenic mice. We also examined its change in mutant SOD1 expressed cells by treatment with proteasome inhibitors. Furthermore, using cells co-expressing mutant SOD1 and Hsp70, we characterized an insoluble SOD1 species influenced by Hsp70 as misfolded proteins. Here we show that SDS-dissociable soluble monomers and SDS-stable soluble dimers of H46R SOD1 appear as early misfolded intermediates in the formation of highly insoluble aggregates, and their levels are coordinately mediated by the proteasome activity and Hsp function.

Materials and methods

Materials. We used the following antibodies: polyclonal human SOD1 antibody (SOD1-100, diluted 0.1 l g/ml, Victoria, BC, Canada); monoclonal antibody against GST-fused full-length human SOD1 protein that specifically binds to human SOD1 (diluted 0.2 l g/ml, MBL, Nagoya, Japan); polyclonal Hsp70 antibody (SPA-757, diluted 1:30,000 for Western blotting, diluted 1:1000 for immunohistochemistry, Stressgen); polyclonal Hsp40 antibody (SPA-400 diluted 1:10,000 for Western blotting, diluted 1:500 for immunohistochemistry, Stressgen). Wild-type SOD1 cDNA fused with an FLAG tag at C-terminus of SOD1 (SOD1-FLAG) was subcloned into either pcDNA3.1 (Invitrogen, Carlsbad, CA, USA) or pEF-BOS vector [20]. Mutant H46R and G93A SOD1 cDNAs were generated by site-directed mutagenesis, and their sequences were confirmed by DNA sequencing. pCMV-Hsp70 and pRC-Hsp40 were described previously [25,26].

Cell culture and transfection. COS-7 and SH-SY5Y cells were grown in Dulbecco's modified Eagle's medium (DMEM, Invitrogen) and a mixture of DMEM and Ham's F-12, respectively, supplemented with 10% fetal bovine serum. SOD1 cDNAs were transfected into cells using Lipofectamine Plus reagents (Invitrogen), according to the manufacturer's protocols [27]. Cultured cells were harvested 48 h after transfection for experiments. For inhibition of the proteasome activity, either MG132 or lactacystin (Sigma, St. Louis, MO, USA) in indicated concentrations was added to cells 24 h after transfection and then cells were further incubated for 24 h. In experiments using Hsp chaperones, either Hsp70 or Hsp40 cDNA was co-transfected with H46R SOD1-FLAG pEF-BOS to COS-7 cells (at a molar ratio of 4:1).

Transgenic mice. Transgenic mouse lines expressing fALS-linked H46R SOD1 under the control of inherent human SOD1 promoter were maintained as hemizygotes by mating with B6/SJF1 as previously described [28]. The transgenic mice expressing wild-type human SOD1 were also kindly supplied by Dr. PH. Chan (Stanford University, Stanford, CA, USA) and maintained as hemizygotes [29]. All of the mouse experiments followed the Guidelines for Animal Experiments of Yamagata University School of Medicine.

Protein fractionation and Western blotting. Protein fractionation of whole mouse spinal cords was performed according to published protocols [30,31] with a slight modification (see Fig. 1A). Whole mouse spinal cords were homogenized by 15 up-and-down strokes with a Teflon homogenizer in 1:3 (wt/vol) phosphate-buffered saline (PBS; 100 mM phosphate, pH 7.4, 150 mM NaCl, and protease inhibitor cocktail (Roche Diagnostics, Mannheim, Germany)). The homogenate was centrifuged at 100,000×g for 20 min at 4 °C, and the resultant supernatant was collected as the PBS-soluble fraction. The pellet was rinsed three times with PBS and was extracted by sonication in 1% Triton X-100 (TX)/PBS. After centrifugation at 100,000×g for 20 min at 4 °C, the supernatant was designated as the TX-soluble fraction. The pellet was washed three times with 1% TX/PBS and extracted by sonication in 5% SDS/PBS. The extract was incubated at room temperature for 30 min and centrifuged at 100,000×g for 20 min at 20 °C. The supernatant was designated as the SDS-soluble fraction. After rinsing and centrifugating three times in 5% SDS/PBS, the resultant pellet was extracted by sonication in 8 M urea/PBS. After centrifugation at 100,000×g for 20 min at 20 °C, the supernatant was designated as the urea-soluble fraction. The pellet was rinsed once with 8 M urea/PBS and extracted by sonication in 88% formic acid (FA). After centrifugation at 100,000×g for 20 min at 20 °C, the supernatant was designated as the FA-soluble fraction. FA was evaporated by SpeedVac (Savant, Farmingdale, NY, USA). After washing the dried pellet with distilled water and lyophilizing it again, the resulting pellet was resuspended by sonication in Laemmli's sample buffer containing 2% SDS and 100 mM dithiothreitol and then boiled for 5 min. The protein concentrations of the PBS-soluble, TX-soluble, SDS-soluble, and urea-soluble fractions were measured by a BCA protein assay (Pierce, Rockford, IL, USA). Cultured cell pellets were fractionated by the same protocol described above until the preparation of the SDS-soluble fraction. The SDS-insoluble pellet was resuspended by sonication in Laemmli's sample buffer and boiled for 5 min. The suspension was designated as the SDS-insoluble fraction.

We performed Western blotting as described previously [27]. All protein samples were boiled for 5 min in Laemmli's sample buffer containing 100 mM dithiothreitol. Ten micrograms of protein from each of the PBS-soluble, TX-soluble, SDS-soluble, and urea-soluble fractions, and equal aliquots of the FA-soluble fraction were loaded on 15% polyacrylamide gels. The relative intensities of detected bands were scanned and quantified with the Scion image program, version 4.02 (Scion Corp., Frederick, MD, USA). Statistical analysis for comparison of groups was performed by ANOVA with Fisher's probability of least significant difference (PLSD) post hoc test for significance using the Statview software version 5 (SAS Institute Inc, Cary, NC, USA).

Immunohistochemistry. The mice, anesthetized with diethyl ether, were sacrificed by transcardial perfusion with 0.9% sodium chloride followed by 4% paraformaldehyde in PBS. The spinal cord was quickly removed, post-fixed with the above solution, and then embedded in paraffin. After deparaffinizing, sections (4-1 m thickness) of the lumbar spinal cord (L_{4-5}) were incubated with 0.3% hydrogen peroxide for 10 min and then with 10% normal goat serum for 30 min. The sections were incubated with the primary antibodies, and they reacted with the appropriate biotinylated secondary antibodies, followed by an avidin-biotin-peroxidase complex (Vector, Burlingame, CA, USA). Color was developed with diaminobenzidine (Sigma).

Results

Mutant-specific alteration of SOD1 solubility in fALS-linked H46R SOD1 transgenic mice

In this study, we used fALS-linked H46R SOD1 transgenic mice as reported previously [28]. To examine the fALS-linked mutation-dependent change of SOD1 solubility, we sequentially extracted spinal cords of mutant transgenic mice with severe motor impairment (~24 weeks of age) with PBS, 1% TX, 5% SDS, 8 M urea, and 88% FA (Fig. 1A), and then separated extracts by SDS–PAGE under the denaturing condition. In 24-week-old non-transgenic littermates and 38-week-old wild-type SOD1

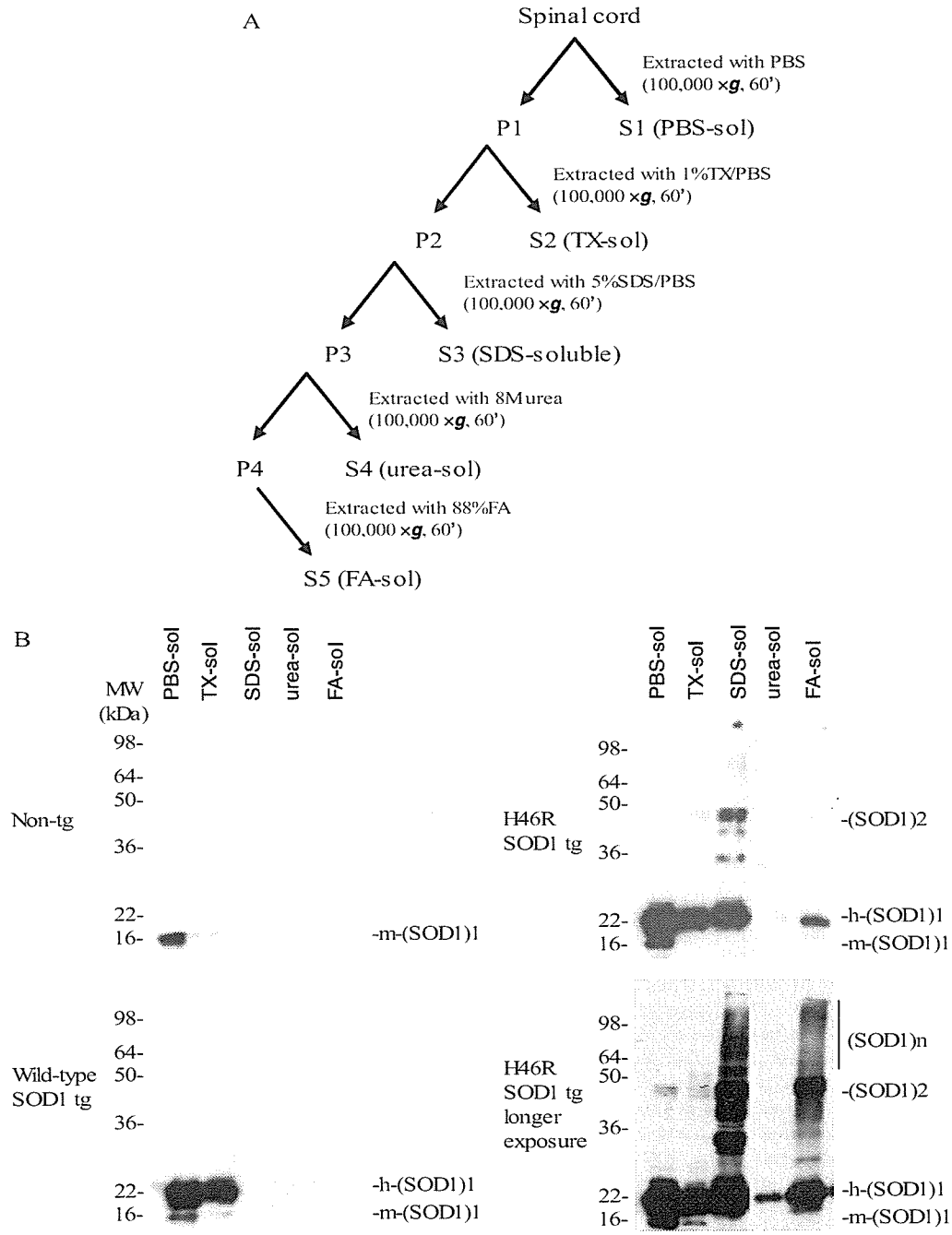

Fig. 1. Mutant-specific alteration of SOD1 solubility in spinal cords from fALS-linked H46R SOD1 transgenic mice. (A) Schematic representation of the sequential extraction steps. (B) Western blot analysis of spinal cords from 24-week-old non-transgenic mice (Non-tg) (upper left panel), 38-week-old wild-type SOD1 transgenic mice (Wild-type SOD1 tg) (lower left panel), and mutant H46R SOD1 transgenic mice at end stage (H46R SOD1 tg) (upper right panel). Ten micrograms of protein from each of the PBS-soluble fraction (PBS-sol), the TX-soluble fraction (TX-sol), the SDS-soluble fraction (SDS-sol), and the urea-soluble fraction (urea-sol) and equal aliquots of the FA-soluble fraction (FA-sol) were subjected to 15% polyacrylamide gels under reducing conditions. Western blots were probed with SOD1-100 antibody, which recognizes both human SOD1 (h-SOD1) and mouse endogenous SOD1 (m-SOD1). The lower right panel (identical to the upper right panel) was exposed to the film for a longer time.

transgenic mice, endogenous mouse SOD1, and wild-type human SOD1 were detected as monomers migrating at 16-kDa and 22-kDa, respectively, in the PBS- and 1% TX-soluble fractions (Fig. 1B). This finding may be explained by the fact that normal SOD1 is a soluble protein located predominantly in the cytosol and less within the membranous organelle such as mitochondrial intermembrane space [4]. In contrast to the control mouse SDS-soluble fraction that was virtually devoid of SOD1, intense bands of SOD1 were found in the SDS-soluble fraction of mutant transgenic mice (Fig. 1B). In the fraction, the anti-SOD1 antibody (SOD1-100) recognized 22-kDa bands ((SOD1)1; it represents SOD1 monomer), ~44-kDa bands ((SOD1)2; apparent molecular weight of (SOD1)2 shows 2-fold to 22-kDa monomer, being consistent with SOD1 dimer as previously reported [19]), and multiple bands above 44-kDa ((SOD1)n; it represents high-molecular-weight (HMW) species). Also, ~28 and ~36-kDa bands were observed in the SDS-soluble fraction. These bands may represent proteolytic fragments from HMW species, but the exact origin was unknown in this study. SOD1 monomers, dimers, and HMW species were further recovered in the FA-soluble fraction, whereas a small amount of monomeric SOD1, but not HMW species, was detected in the urea-soluble fraction, indicating that FA-soluble SOD1 species were not simply carried over from the prior urea extracts (Fig. 1B). TX-insoluble/SDS-soluble (designated as SDS-soluble) species are characterized by an alteration of solubility to distinguish mutant H46R SOD1 from a wild-type one. Also, mutant H46R SOD1 contained SDS-stable oligomers with diverse solubility in detergents or denaturants.

Age-dependent alteration of SOD1 solubility in H46R SOD1 transgenic mice

As described in our previous report, the H46R SOD1 transgenic mice showed motor dysfunction with aging, and the stages of motor dysfunction could be classified into four time periods based on the Rotarod test: 13 weeks, 17 weeks, 21 weeks, and later 23 weeks of age were designated as the early presymptomatic stage (EP), late presymptomatic stage (LP), symptomatic stage (SS), and end stage (ES), respectively [28]. To clarify the alteration of SOD1 solubility with aging in mutant SOD1 transgenic mice, we compared the levels of SOD1 species, which were biochemically fractionated as described above, in the different stages (Figs. 2A and B). The levels of both PBS-soluble and TX-soluble SOD1 monomers showed no statistically significant difference between stages, although they had a tendency to decrease with aging (Figs. 2A and B). In the SDS-soluble fraction, mutant SOD1 monomers and dimers were clearly detected at EP. The ratios of SOD1 monomers at EP and LP versus ES were $20.52 \pm 6.41\%$ (mean $\pm$ SD) and $45.88 \pm 2.30\%$, respectively. In addition, the ratios of SOD1 dimers at EP and LP versus ES were $29.38 \pm 21.20\%$ and $68.47 \pm 10.27\%$, respectively. On the other hand, the levels of SOD1 HMW species showed the later elevation at the period between LP and SS. These findings indicate that the increase of SDS-dissociable soluble SOD1 monomers and SDS-stable soluble SOD1 dimers occurred between EP and LP before onset ($n = 3$, $p = 0.017$ and $p = 0.005$, respectively) (Fig. 2B). In the FA-soluble fraction, a small number of SOD1 monomers were also seen at EP, but there was no significant difference in the levels of monomers between EP and LP. The ratios of SOD1 monomers at LP and SS versus ES were $32.31 \pm 12.99\%$ and $68.30 \pm 17.03\%$, respectively. The ratios of SOD1 dimers at LP and SS versus ES were $12.73 \pm 6.27\%$ and $41.42 \pm 4.50\%$, respectively. The levels of FA-soluble SOD1 monomers and FA-soluble dimers significantly increased between LP and SS ($p = 0.036$ and $p < 0.001$, respectively), while the levels of FA-soluble SOD1 HMW species elevated later in the period between SS and ES (Figs. 2A and B). The levels of SDS-dissociable soluble monomers and SDS-stable soluble dimers elevated earlier than the SDS-stable soluble HMW species and FA-soluble species.

To examine the relation between the alteration of SOD1 solubility and the formation of SOD1-inclusions with aging, we immunostained mouse spinal cords in four different stages with monoclonal anti-SOD1 antibody (Fig. 2C). At EP, we did not detect any kind of SOD1-inclusions. SOD1-inclusions in the neuropil appeared at SS, and the number of SOD1-inclusions increased between SS and ES (Fig. 2C). SOD1-inclusions increased after disease onset, indicating that the accumulation of SDS-dissociable soluble SOD1 monomers and SDS-stable soluble dimers precedes the appearance of SOD1-inclusions.

The increase of Hsp70/40 in the SDS-soluble fraction with aging in H46R SOD1 transgenic mice

To examine how the mutant-specific alteration of SDS solubility is associated with the molecular chaperone system, the fractionated samples prepared above were analyzed by Western blotting using antibodies to Hsp70 and Hsp40. Hsp70 and Hsp40 were found to be rich in the PBS-soluble and the TX-soluble fractions (Fig. 3A). PBS- and TX-soluble Hsp70 and Hsp40 showed constant levels in all stages of mutant transgenic mice and were not different from those in 24-week-old non-transgenic littermates and 38-week-old wild-type SOD1 transgenic mice (Fig. 3A). In the SDS-soluble fraction, the levels of Hsp70 and Hsp40 in mutant transgenic mice at LP were higher than those in the control mice at later 24 weeks of age. The levels of Hsp70 and Hsp40 in the SDS-soluble fractions elevated at the period between EP and LP in mutant transgenic mice (Fig. 3A). To clarify how the increase of Hsp70 and Hsp40 in the SDS-soluble fraction reflects in histopathological change with aging, we immunostained the lumbar spinal cords with antibodies to Hsp70 and Hsp40 (Fig. 3B). SOD1-positive inclusions were intensely stained with the antibody to Hsp70 as previously reported and faintly reacted with the antibody to Hsp40 in

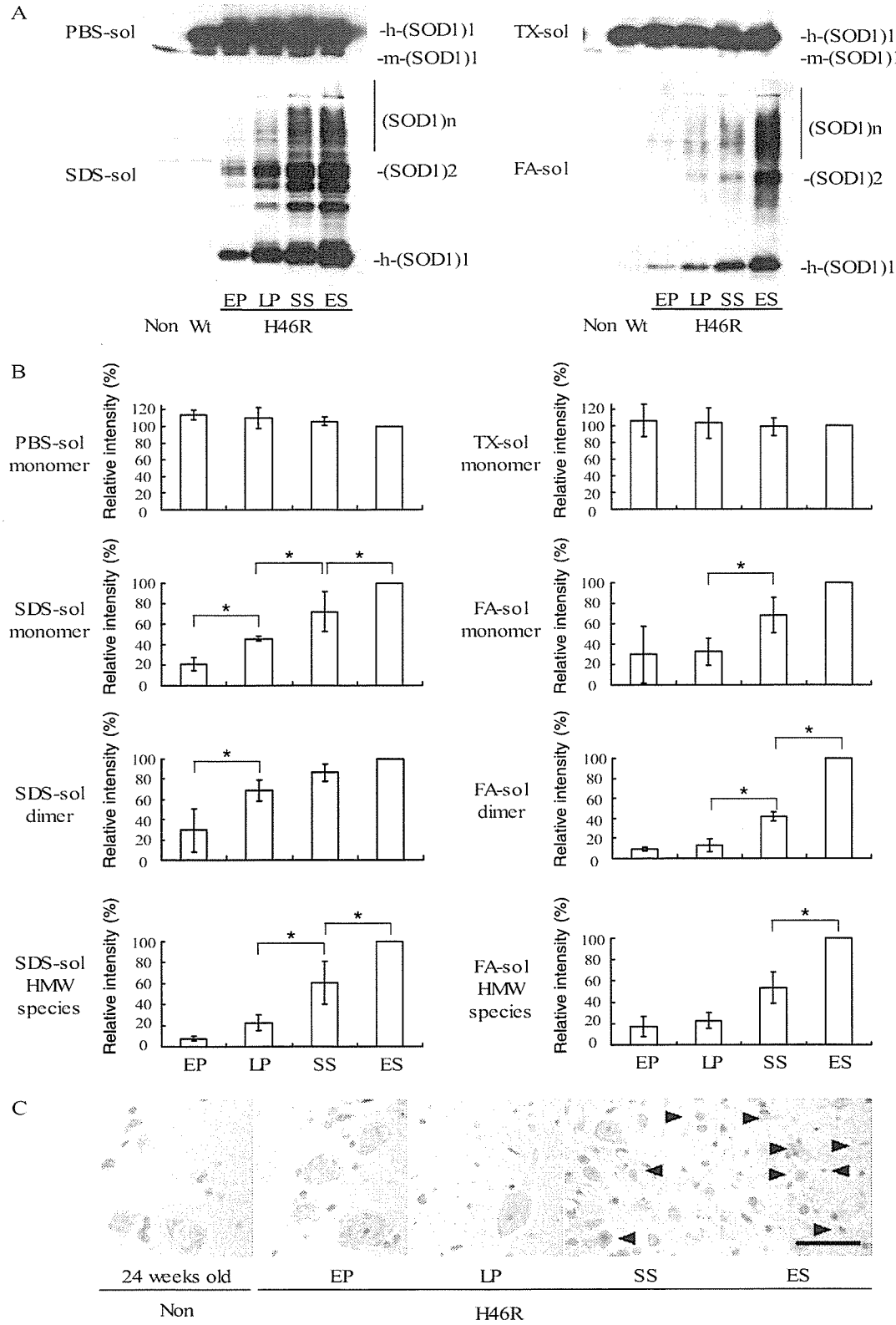

Fig. 2. Age-dependent alteration of SOD1 in spinal cords from H46R SOD1 transgenic mice. (A) The spinal cords of 24-week-old non-transgenic littermates (Non), 38-week-old wild-type SOD1 transgenic mice (Wt), and H46R SOD1 transgenic mice (H46R) at early presymptomatic stage (EP), late presymptomatic stage (LP), symptomatic stage (SS), and end stage (ES) were sequentially fractionated. Ten micrograms of protein from each of the PBS-soluble fraction (PBS-sol), the TX-soluble fraction (TX-sol), and the SDS-soluble fraction (SDS-sol), and equal aliquots of the FA-soluble fraction (FA-sol) were loaded on the gel and then immunoblotted with SOD1-100 antibody. (B) The graphs represent relative intensities of H46R SOD1 species at each stage (n = 3, bars represent mean ± SD, *$P < 0.05$). (C) Immunohistochemical analysis of lumbar spinal cords (L_{4-5}) of 24-week-old non-transgenic littermates (Non) and H46R SOD1 transgenic mice (H46R) at four stages. These sections were immunostained with monoclonal anti-SOD1 antibody specific to human SOD1. Scale bars = 50 μm. Arrowheads indicate SOD1-immunoreactive structures.

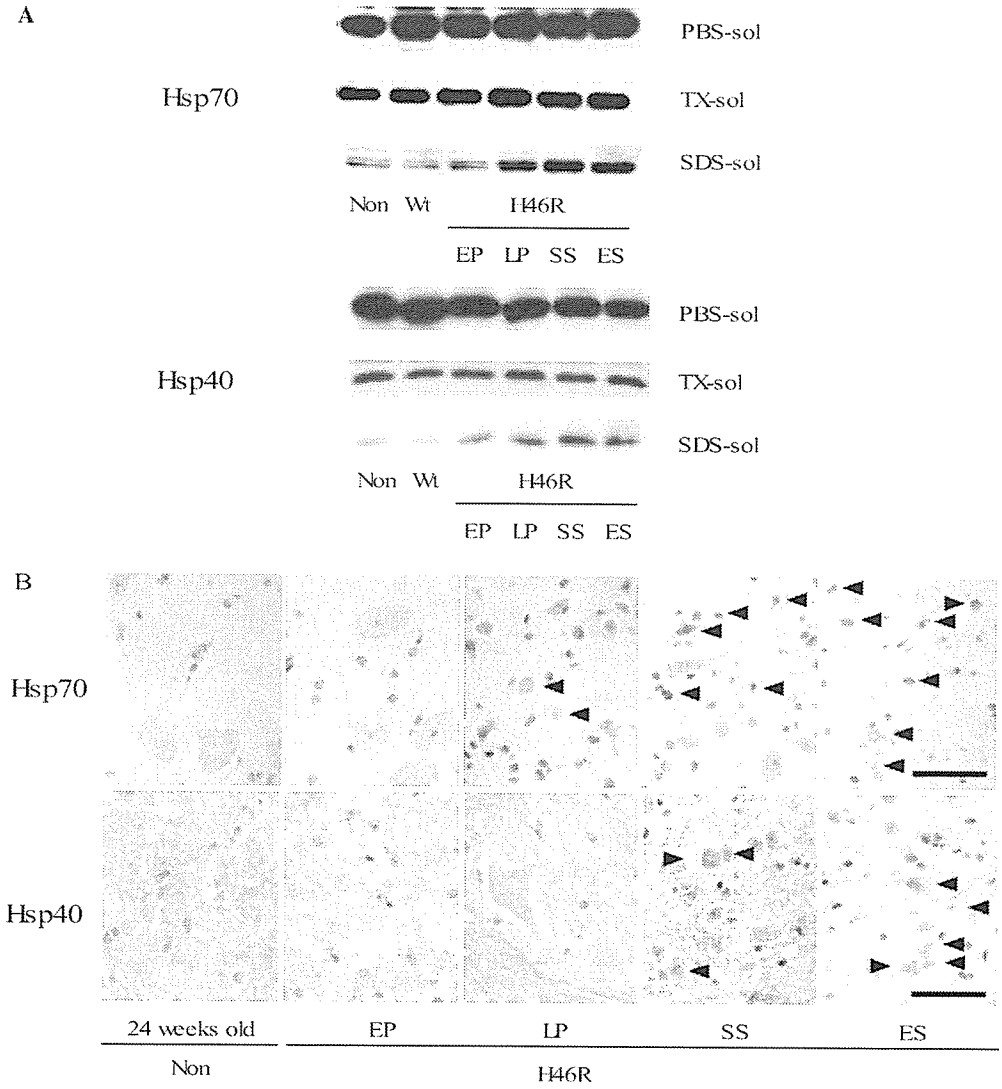

Fig. 3. (A) Increase of Hsp70 and Hsp40 in the SDS-soluble fraction from H46R SOD1 transgenic mice. The fractionated samples used in Fig. 2 were analyzed by Western blotting using anti-Hsp70 and anti-Hsp40 antibodies. Ten micrograms of total protein from each fraction was loaded on each lane. (B) Time course analysis of Hsp-immunoreactive structures. These sections were immunostained with anti-Hsp70 antibody and anti-Hsp40 antibody. Scale bars = 50 l m. Arrowheads indicate immunoreactive structures of each antibody.

the serial sections (data not shown). Although a small number of Hsp70-positive structures were found in neuropil at LP, the increase of SOD1-inclusions containing Hsp70 immunoreactivities was remarkable after SS (Fig. 3B). Similarly, Hsp40-positive structures increased from SS (Fig. 3B). The present data showed that the increase of Hsp70 and Hsp40 in the SDS-soluble fraction appeared along with the increase of SDS-dissociable soluble SOD1 monomers and SDS-stable soluble dimers. This increase of Hsp70 and Hsp40 occurred before the accumulation of visible inclusions with Hsp70 and Hsp40 immunoreactivities.

Inhibition of the proteasome activity promotes the change of SOD1 solubility in cells expressing H46R SOD1

The fALS-linked mutant misfolded SOD1 protein is reported to be degraded by the proteasome pathway [16,17,19,20]. To see how inhibition of the proteasome pathway influences mutant SOD1 solubility, we examined COS-7 cells transiently overexpressing either wild-type SOD1-FLAG or H46R SOD1-FLAG in the presence or absence of proteasome inhibitor MG132. In this experiment, FLAG-tagged SOD1 was used for discriminating exogenous SOD1 from endogenous SOD1 by migrating more slowly. Collected cell pellets were sequentially extracted with PBS, 1% TX, and 5% SDS. In the PBS-soluble and the TX-soluble fractions, the levels of mutant SOD1 as well as wild-type SOD1 slightly increased when MG132 was added in a dose-dependent manner (Fig. 4A). In the SDS-soluble fraction, a small amount of wild-type monomeric SOD1 was seen in the absence of MG132. The levels of wild-type SOD1 monomers increased without generating HMW species in the presence of 10 l M MG132. On the other hand, in the SDS-soluble fraction, mutant SOD1 monomers and dimers were obviously

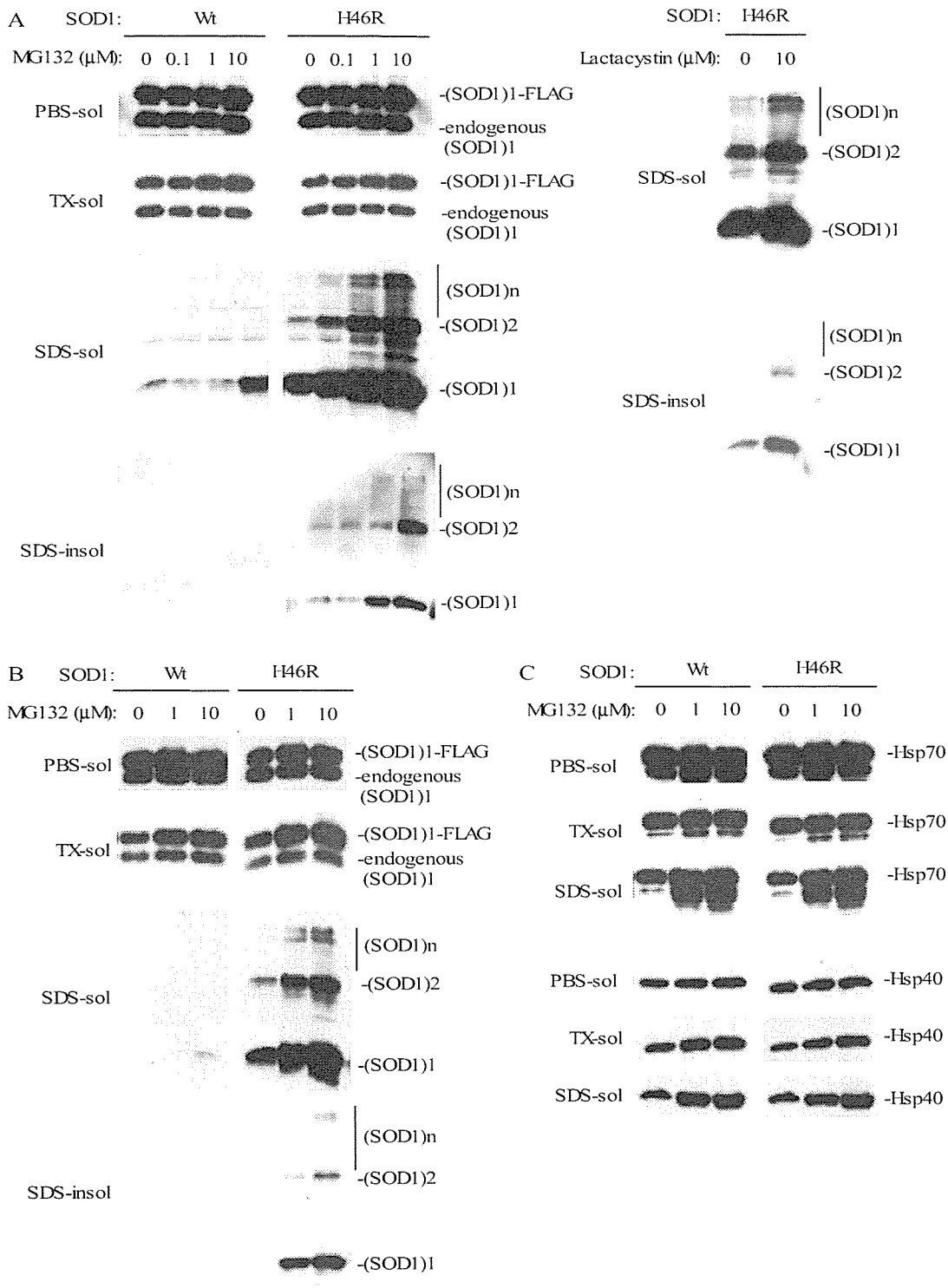

Fig. 4. Alteration of H46R SOD1 solubility in COS-7 and SH-SY5Y cells by treatment with proteasome inhibitors. COS-7 cells (A) and SH-SY5Y cells (B,C) were transiently transfected with either wild-type SOD1-FLAG pcDNA3.1 or H46R SOD1-FLAG pcDNA3.1. At 24 h after transfection, the culture medium was replaced with a fresh one containing the indicated concentrations of proteasome inhibitor, either MG132 (left panels of (A) and all panels of (B)) or lactacystin (right panels of (A)). Cells were incubated for an additional 24 h. Collected cell pellets were serially fractionated to the PBS-soluble fraction (PBS-sol), the TX-soluble fraction (TX-sol), the SDS-soluble fraction (SDS-sol), and the SDS-insoluble fraction (SDS-insol). Ten micrograms of protein from each of the PBS-soluble fraction, the TX-soluble fraction, and the SDS-soluble fraction, and equal aliquots of the SDS-insoluble fraction were subjected to the gel and immunoblotted with SOD1-100 (A,B). (C) The levels of both endogenous Hsp70 and Hsp40 were elevated in the SDS-soluble fraction from cells expressing wild-type SOD1 as well as mutant SOD1 in an MG-132 dose-dependent manner. The fractionated samples used in (B) were analyzed by Western blotting using anti-Hsp70 and anti-Hsp40 antibodies.

detected in the absence of MG132 and showed a significant increase in generating HMW species by treatment with MG132 in a dose-dependent manner (Fig. 4A). Similarly, in the SDS-insoluble fraction, the levels of mutant SOD1 monomers, dimers, and HMW species elevated by treatment with MG132 in a dose-dependent manner, while wild-type SOD1 was not detected (Fig. 4A). Dose-dependent treatment with MG132 further showed that the elevation of SDS-dissociable soluble mutant SOD1 monomers and SDS-stable soluble dimers preceded that of SDS-stable soluble HMW species and SDS-insoluble species. Treatment with another specific proteasome inhibitor, lactacystin, also caused the accumulation of SDS-soluble and SDS-insoluble mutant SOD1 species in COS-7 cells, although to a lesser extent (Fig. 4A). We further confirmed the effect of MG132 on the alteration of SOD1 solubility in human neuroblastoma SH-SY5Y cells. By treatment with MG132, SDS-soluble and SDS-insoluble mutant SOD1 monomers, dimers, and HMW species accumulated in mutant-specific and dose-dependent manners in SH-SY5Y cells similar to COS-7 cells (Fig. 4B). The elevation of SDS-dissociable soluble mutant SOD1 monomers and SDS-stable soluble dimers also preceded that of SDS-stable soluble HMW species and SDS-insoluble species. In SH-SY5Y cells expressing mutant SOD1, the levels of both endogenous Hsp70 and Hsp40 were elevated in the SDS-soluble fraction in an MG-132 dose-dependent manner (Fig. 4C). However, the increase of endogenous Hsp70 and Hsp40 levels in the SDS-soluble fraction was similarly observed in cells expressing wild-type SOD1 (Fig. 4C). These results showed that inhibition of the proteasome activity in mutant SOD1 expressed cells recapitulated the alteration of SOD1 solubility with aging in mutant transgenic mice. Inhibition of the proteasome activity initially led to the accumulation of SDS-dissociable soluble mutant SOD1 monomers and SDS-stable soluble dimers prior to that of SDS-stable soluble HMW species and SDS-insoluble species irrespective of the increase of endogenous Hsp70 and Hsp40.

Effect of overexpression of Hsp70 on the accumulation of SDS-soluble and SDS-insoluble mutant SOD1 species

Overexpression of Hsp70 has been reported to reduce the SOD1-aggregate formation and prolong cellular viability in a cellular model of fALS [23]. As described in our previous report [20], overexpression of mutant SOD1 pEF-BOS in COS-7 cells causes higher expression levels of SOD1 than overexpression of mutant SOD1 pcDNA3.1, and a large amount of SDS-insoluble mutant SOD1 appears without adding proteasome inhibitor. By taking advantage of this high-expression system, we investigated cells co-transfected with mutant H46R SOD1 cDNA and a 4-fold molar excess of Hsp cDNA to see the effect of Hsp70 and Hsp40 on the levels of altered insoluble SOD1 species (Fig. 5A). Overexpression of Hsp70 obviously reduced the levels of SDS-dissociable soluble mutant SOD1 monomers, SDS-stable soluble dimers, and SDS-stable soluble HMW species, compared to co-expression of the empty vector (Fig. 5A). Overexpression of Hsp40 showed a weaker effect on the levels of SDS-soluble mutant SOD1 species (Fig. 5A). Co-overexpression with Hsp70 plus Hsp40 enhanced the effect of Hsp70 on a decrease of the levels of SDS-stable soluble mutant SOD1 dimers and HMW species (Fig. 5A). In the SDS-insoluble fraction, overexpression of Hsp70 also led to a reduction in the levels of SDS-dissociable insoluble mutant SOD1 monomers, SDS-stable insoluble dimers, and SDS-stable insoluble HMW species, and the effect was enhanced by co-overexpression of Hsp40 (Fig. 5A). This finding was also observed in cells expressing different fALS-linked mutant G93A SOD1 (data not shown). To further examine the molecular mechanism by which overexpression of Hsp70 reduced insoluble mutant SOD1 species, cells were co-transfected with H46R SOD1 and Hsp70 cDNAs in various molar ratios (Fig. 5B). The levels of mutant SOD1 monomers, dimers, and HMW species in the SDS-soluble fraction as well as in the SDS-insoluble fraction decreased in negative correlation to the amounts of transfected Hsp70 cDNA (Figs. 5B and C). On the other hand, the levels of mutant SOD1 monomers in the PBS-soluble and TX-soluble fractions did not increase, in sharp contrast to the significant reduction of the amount of SDS-soluble species by overexpression of Hsp70 (Figs. 5B and C). These findings demonstrated that overexpressed Hsp70 modulated the levels at SDS-dissociable soluble mutant SOD1 monomers and SDS-stable soluble dimers as misfolded proteins and preferentially forwarded abnormally insoluble SOD1 species to degradation rather than to refolding.

Discussion

Although wild-type SOD1 is principally a soluble, cytosolic protein [4], fALS-linked mutant SOD1 has a tendency to assemble as insoluble aggregates, which are immunohistochemically observed as cytoplasmic inclusions in patients with fALS having SOD1 mutation [10]. There has been controversy about whether such inclusions are a cause or simply a result of the neuronal degeneration. Immunohistochemical experiments do not rule out the possibility that mutant SOD1 aggregates can damage motor neurons, even though microscopically visible inclusions are absent in the early period. In agreement with the previous finding [16,19], our immunohistochemical data demonstrated that SOD1-positive inclusions appeared after disease onset, and the accumulation of SOD1-positive inclusions was parallel to the elevation of most insoluble SOD1 species recovered in the FA-soluble fraction. On the other hand, we revealed that mutant H46R SOD1 began to significantly alter its solubility to SDS-dissociable soluble monomers and SDS-stable soluble dimers earlier than the appearance of visible SOD1-positive inclusions. These findings suggest that complexes of SDS-dissociable soluble SOD1 monomers and SDS-stable soluble dimers were much smaller in